NASA GRANT NAG-1-244

NUMERICAL SOLUTIONS OF THE COMPLETE NAVIER-STOKES EQUATIONS

Progress Report No. 27

For the Period October 1, 1995 to September 30, 1996

Prepared by

H. A. Hassan
Project Coordinator

Department of Mechanical and Aerospace Engineering
Post Office Box 7910
North Carolina State University
Raleigh, North Carolina 27695-7910

During this period, three papers were presented[1-3] (copies enclosed) and three abstracts were accepted for the 97 AIAA Sciences Meeting and Exhibit to be held at Reno in January, 1997.

Progress is being made on a number of fronts. We have developed a k-ζ (Enstrophy) model capable of predicting turbulence separation and applied it to two airfoils: NACA 0012 and RAE 2822 at various angles of attack and Mach numbers. Moreover, a two-equation k-ζ model with a tensor eddy viscosity has been developed. The goal of this work is to eliminate the empirical damping factor, f_μ, that is used in defining the eddy viscosity in wall bounded flows. Plans call for this model to be used in calculating three dimensional turbulent flows.

The work on compressible turbulence is progressing well. Current efforts are devoted to analyzing crossing shocks interaction with turbulent boundary layers.

Finally, we have developed an alternative to the e^n method using models similar to those employed in turbulence modeling. The method was implemented into boundary layer codes and is being incorporated into a Navier-Stokes solver. As a result of this method, the onset of transition and the rest of the flowfield can be obtained from a single Navier-Stokes code.

References

1. Alexopoulos, G. A. and Hassan, H. A., "A k-ζ (Enstrophy) Compressible Turbulence Model for Mixing Layers and Wall bounded Flows," AIAA Paper 96-2039, June 1996.
2. Robinson, D. F. and Hassan, H. A., "A Two-Equation Turbulence Closure Model for Wall Bounded and Free Shear Flows," AIAA Paper 96-2057, June 1996.
3. Rao, M. S. and Hassan, H. A., "Modeling Turbulence in the Presence of Adverse Pressure Gradients," AIAA Paper 96-2429, June 1996.

AIAA 96-2429
Modeling Turbulence in the Presence of Adverse Pressure Gradients

Mahesh S. Rao
North Carolina State University
Raleigh, NC

H. A. Hassan
North Carolina State University
Raleigh, NC

14th AIAA Applied Aerodynamics Conference

June17-20, 1996 / New Orleans, LA

MODELING TURBULENCE IN THE PRESENCE OF ADVERSE PRESSURE GRADIENTS

M. S. Rao* and H. A. Hassan†
North Carolina State University, Raleigh, North Carolina 27695-7910

Abstract

In an attempt to model a recent set of experiments by Skare and Krogstad dealing with equilibrium boundary layers near separation, it became clear that the traditional k-ω model was unable to reproduce the data. Careful investigation of the data suggested that the diffusion term in the k - equation behaves differently in the presence and absence of unfavorable pressure gradients. This led to the conclusion that an important diffusion mechanism was missing from the k - equation and a new diffusion model was proposed. The results of the new theory indicate marked improvement when compared with the data for strong adverse pressure gradient flows. Moreover, the new theory reproduces Stratford's limit of velocity in a region of vanishing shear stress. However, because subsonic and supersonic boundary layers act differently in the presence of an adverse pressure gradient, no adjustments in the diffusion term is recommended for supersonic flows in the presence of mild adverse pressure gradients.

Introduction

It is a known fact that traditional turbulence models are somewhat inadequate when it comes to predicting flows with an adverse pressure gradient[1]. This is a result of prevailing modeling practices. Whether we deal with one-equation, two-equation, or a stress model, current modeling does not address situations where adverse pressure gradients play a role. Thus, we use results from the decay of homogeneous turbulence, the log-law region, and asymptotic expansions along turbulent-non-turbulent boundaries to determine model constants[1]. There is no reason to expect that such practices will produce turbulence models that are valid in the presence of unfavorable pressure gradients.

The situation has changed recently with the availability of well documented incompressible experiments describing equilibrium boundary layers near separation[2,3]. As is shown in Ref. 3, the diffusion term in the k - equation behaves differently in the presence and absence of pressure gradients. This led us to the conclusion that an important diffusion mechanism is missing from the k - equation.

The objective of this investigation is to show that there is indeed a missing term resulting from the traditional neglect of the term $\overline{p'u_i'}$, where p' and u_i' are the pressure and velocity fluctuations. Moreover, it results in improved agreement between theory and experiment for low speed flows.

However, subsonic and supersonic boundary layers are known[4] to behave differently in the presence of adverse pressure gradients. As a result, a modification like the one suggested here is not expected to apply for all Mach numbers. It has been suggested that compression associated with an adverse pressure gradient is associated with an increase in skin friction and a decrease in boundary layer thickness at supersonic speeds. This would suggest that some modification of the proposed turbulence model is required. While examining the experiment of Fernando and Smits[5], we discovered that a traditional k-ω model was quite satisfactory. As a result, it is concluded that adjustment in the diffusion term is only required for subsonic flows.

Analysis

The application of an adverse pressure gradient on a wall bounded flow promotes separation of the boundary layer. Thus, we use the theoretical behavior of turbulent boundary layers near separation to investigate current modeling practice.

The only term that requires modeling in the k - equation is the diffusion term[1]. Traditionally, it is modeled as

$$\frac{1}{2}\rho\overline{u_i'u_i'u_j'} + \overline{p'u_j'} = -\mu_t\sigma^*\frac{\partial k}{\partial x_j} \qquad (1)$$

---

* Research Assistant, Mechanical and Aerospace Engineering, Student Member AIAA.

† Professor, Mechanical and Aerospace Engineering, Associate Fellow AIAA.

where ρ is the density, k is the turbulent kinetic energy, μ_t is the turbulent viscosity, and σ^* is a model constant.

The applicability of this model near separation is evaluated for an incompressible flow. In the near wall region, the Wilcox k-ω model reduces to

$$0 = -\frac{\partial P}{\partial x} + \frac{\partial \tau}{\partial y} \tag{2}$$

$$0 = \frac{\partial}{\partial y}\left[\sigma^* \nu_t \frac{\partial k}{\partial y}\right] + \nu_t \left(\frac{\partial U}{\partial y}\right)^2 - \beta^* \omega k \tag{3}$$

$$0 = \frac{\partial}{\partial y}\left[\sigma \nu_t \frac{\partial \omega}{\partial y}\right] + \alpha \left(\frac{\partial U}{\partial y}\right)^2 - \beta \omega^2 \tag{4}$$

where the turbulent viscosity is defined as

$$\nu_t = \frac{k}{\omega}, \tag{5}$$

P is the pressure, τ is the shear stress, k is the turbulent kinetic energy, and ω is the specific dissipation rate. The values of the model constants are

$$\alpha = \frac{5}{9}, \qquad \beta = \frac{3}{40}, \qquad \beta^* = \frac{9}{100} \tag{6}$$

$$\sigma^* = \frac{1}{2}, \qquad \sigma = \frac{1}{2} \tag{7}$$

Integration of Eq. (2) gives

$$\tau = \tau_w + y\frac{\partial P}{\partial x} = \mu_t \frac{\partial U}{\partial y} \tag{8}$$

where τ_w is the wall shear stress. In regions where $\tau_w \to 0$, Stratford[6] showed that U has the form

$$U = 2\left(\sqrt{P'y}\right)/K_o, \qquad P' = \frac{1}{\rho}\frac{\partial P}{\partial x} \tag{9}$$

where K_o is typically a constant of about 0.5. Equation (9) was later confirmed by Townsend[7] using the data of Schubauer and Klebanoff[8].

The velocity gradient given by Eq. (9) is

$$\frac{\partial U}{\partial y} = \frac{1}{K_o}\left(\frac{P'}{y}\right)^{\frac{1}{2}} \tag{10}$$

Applying Eqs. (9) and (10) to Eq. (8) in the limit of vanishing shear stress yields

$$\nu_t = K_o P'^{\frac{1}{2}} y^{\frac{3}{2}} \tag{11}$$

When Eqs. (9), (10), and (11) are substituted into Eqs. (3) and (4), the system yields two equations in two unknowns. Solution of these equations reveals the asymptotic behavior in the region near separation. The general procedure entails setting

$$k = Ay^m, \quad \omega = By^n \tag{12}$$

where A and B are functions of P'. Eq. (3) becomes

$$0 = m\left(m + \frac{1}{2}\right) A\sigma^* K_o P'^{\frac{1}{2}} y^{m-\frac{1}{2}} + \frac{1}{K_o} P'^{\frac{3}{2}} y^{\frac{1}{2}} - \beta^* A B y^{m+n} \tag{13}$$

If Eq. (13) is independent of y, then

$$m - \frac{1}{2} = \frac{1}{2} = m + n \tag{14}$$

resulting in

$$m = 1, \qquad n = -\frac{1}{2} \tag{15}$$

Thus, Eqs. (5), (11), (12), and (15) give

$$\frac{A}{B} = K_o P'^{\frac{1}{2}} \tag{16}$$

Substituting above into Eq. (4) yields

$$0 + \frac{\alpha P'}{K_o^2 y} - \frac{\beta B^2}{y} = 0 \tag{17}$$

which simplifies to

$$B = \frac{1}{K_o}\left(\frac{\alpha}{\beta}\right)^{\frac{1}{2}} P'^{\frac{1}{2}} \tag{18}$$

which gives

$$A = \left(\frac{\alpha}{\beta}\right)^{\frac{1}{2}} P' \tag{19}$$

When Eqs. (15), (18), and (19) are applied to Eq. (13), one finds

$$\frac{3}{2}\left(\frac{\alpha}{\beta}\right)^{\frac{1}{2}}\sigma^* K_o + \frac{1}{K_o} - \frac{\alpha\beta^*}{K_o^2\beta} = 0 \qquad (20)$$

Noting that

$$\alpha\frac{\beta^*}{\beta} = \frac{2}{3} \qquad (21)$$

from the values of the constants, Eq. (20) reduces to

$$\frac{3}{2}\left(\frac{\alpha}{\beta}\right)^{\frac{1}{2}}\sigma^* K_o + \frac{1}{3K_o} = 0 \qquad (22)$$

In view of Eq. (13), the above result is a contradiction. This shows that the current modeling of diffusion is inadequate in a region near separation.

To remedy the above situation, we supplement diffusion with an additional term. The proposed modeling of the diffusion term is

$$\frac{1}{2}\rho\overline{u_i' u_i' u_j'} + \overline{p' u_j'} = -\mu_t\left[\sigma^*\frac{\partial k}{\partial x_j} + \sigma_p^*\frac{b_{ij}\partial P}{\rho\,\partial x_j}\right] \qquad (23)$$

where

$$b_{ij} = \frac{\tau_{ij}}{\rho k} + \frac{2}{3}\delta_{ij}, \qquad \tau_{ij} = -\rho\overline{u_i' u_j'} \qquad (24)$$

and σ_p^* is a model constant. This model constant is determined from the same analysis performed above. Using the standard k - ω notation, it can be shown that

$$\sigma_p^* = -\sigma^*\left(\frac{\alpha}{\beta}\right) - \frac{2}{9K_o^2}\left(\frac{\alpha}{\beta}\right)^{\frac{1}{2}} \cong -6.03 \qquad (25)$$

for $K_o = 0.51$. The value of K_o was found by Townsend[7] based on the data of Schubauer and Klebanoff[8]. Note that σ_p^* is negative, so the new term is a negative diffusion term in the near wall region for an adverse pressure gradient. It should be pointed out that the Stratford limit is valid in the near-wall region where $\tau_w \to 0$. The flow under consideration is attached. Thus the value presented in Eq. (25) is to be treated as a crude estimate of σ_p^*. After computations were made for a strong adverse pressure gradient flow, we set $\sigma_p^* = -5.13$ to best match the experiment.

It should be noted that Saffman[9] attempted to reproduce the above limit using his k - ω^2 model. He found that in order for his model to reproduce Eq. (9), the various flow parameters must take on imaginary values. The same can be shown for the k - ε model.

Results and Discussion

A boundary layer code[10] is employed in carrying out the computations. A standard k - ω model and a modified k - ω model were implemented. A k - ω model and not a k - ε was selected because it has been found[11] that a k - ω model performs better in the presence of adverse pressure gradients. Detailed data on the conditions of Ref. 2 and Ref. 5 were used to test the turbulence models. These experiments will be denoted Experiment (1) and Experiment (2), respectively.

Experiment (1)

Experiment (1) reports an equilibrium boundary layer in a strong adverse pressure gradient flow at a Reynolds number per length of approximately 1.2 million. An equilibrium flow exhibits similarity in the outer region of the boundary layer[7]. The equilibrium region is maintained between $x_c = 4$ m and $x_c = 5$ m. Figure 1 plots the pressure coefficient distribution for this case. The strength of the pressure gradient is measured by the nondimensional pressure gradient parameter

$$\beta_T = \frac{\delta^*\partial P}{\tau_w \partial x} \qquad (26)$$

where δ^* is the displacement thickness. An average value of $\beta_T = 20$ was maintained in the equilibrium region.

A zero pressure gradient flat plate boundary layer is used to match Re_θ, the momentum thickness Reynolds number, in the test section. Figure 2 plots the computed and experimental Reynolds numbers based on the length scales. Good agreement is maintained with the integral length scales.

In order to mimic the conditions stipulated by Stratford, the added diffusion term was implemented in the boundary layer code as

$$\chi H(\chi) \qquad (27)$$

where

$$\chi = \frac{\partial}{\partial x_i}\left[\mu_t\frac{b_{ij}\partial P}{\rho\,\partial x_j}\right] = \frac{\partial}{\partial y}\left(\frac{k}{\omega^2}\frac{\partial U}{\partial y}\frac{\partial P}{\partial x}\right) \qquad (28)$$

$H(\chi)$ is the Heaviside function, *i.e.* $H(\chi) = 1$ for $\chi > 0$ and zero otherwise.

Skin friction values are compared in Figure 3. Skin friction is defined as

$$C_{f,e} = \frac{\tau_w}{\frac{1}{2}\rho_e U_e^2} \tag{29}$$

where $(\ )_e$ denotes a quantity based on boundary layer edge values. k-ω results are about 50% larger than the expected results. The new model matches the data quite well with only a slight underprediction in the equilibrium pressure region of approximately 10%.

The mean velocity profiles are compared in Figures 4 and 5 with the law of the wall, where

$$U^+ = \frac{U}{u_\tau}, \qquad y^+ = \frac{(y u_\tau)}{\nu} \tag{30}$$

where ν denotes the kinematic viscosity and the friction velocity is defined as

$$u_\tau = \sqrt{\frac{\tau_w}{\rho}} \tag{31}$$

The data and the new model results match quite well, whereas the k-ω model underpredicts the profiles. The log law maintains its validity in adverse pressure gradient flows for a range of y^+. The pressure gradient affects the point of departure from the log law.

Figure 6 plots the shear stress in the boundary layer at all six measurement stations. The peak of the shear stress is at approximately $y/\delta = 0.5$. In a zero pressure gradient flow, the maximum shear stress is at the wall. Similar behavior was found in other adverse pressure gradient flow cases.[5,8,12] The modified k-ω results match the data quite well for $y/\delta \le 0.5$ and only slightly overpredicts the outer region. Both methods find the correct location of the peak, but the magnitude is consistently underpredicted by the k-ω model.

Based on these results, we notice that τ_w, as determined by the original k-ω model, is greatly over-estimated in regions of strong adverse pressure gradients. In such regions, the velocity distribution described by Stratford for vanishing shear stress adequately describes the near wall behavior and thus matches the skin friction.

Experiment (2)

Experiment (2) consists of data from an adverse pressure gradient, supersonic turbulent flow on a flat plate. At the start of the test section, the reference Mach number is $M_{ref} = 2.92$. A fit of the wall pressure is shown in Figure 7. The maximum $\beta_T = 5.8$ in this pressure field, much lower than the values found in Experiment (1). As before, a zero pressure gradient flat plate boundary layer is used to match the initial conditions. Emphasis was placed on matching Re_{δ^*} at the start of the of the pressure gradient. The error for Re_{δ^*}, Re_δ, and Re_θ are 0%, 2%, and 17% at the start of the test section.

The skin friction predictions from both models are compared to the data in Figure 8. The skin friction is defined here as

$$C_{f,ref} = \frac{\tau_w}{\frac{1}{2}\rho_{ref} u_{ref}^2} \tag{32}$$

where $(\ )_{ref}$ denotes the reference values at $x_c = 1$. The wall shear stress is determined by the authors based on the Bradshaw and Unsworth[13] calibration of a Preston probe, and also by solving for the friction velocity based on either a Van Driest[14] or a Carvin *et al.*[15] velocity transformation. The three methods agree within 6% of each other. The k-ω model outperforms the new model and matches the data well. The new model underpredicts the skin friction by almost 22%.

The typical mean velocity profile is plotted in Figure 9. The k-ω model matches the profile in the near wall region better than the present model. However, in the outer region, both methods under-predict the slope for the velocity rise. The mean density profile is compared with the theory in Figure 10 for the same location. Both models overestimate the density increase in the near wall region and the final density value at the edge of the boundary layer.

Figure 11 displays the calculated and experimental shear stress for two locations. A dramatic difference between the two models is seen at $x_c = 1.254$. The standard k-ω model follows the data trend in the outer region well, but overshoots the data peak by approximately 18%, which is within -5% to 30% uncertainty associated with these data. Also note that for $y/\delta < 0.5$, the data is considered problematic. The current model misses the proper trend from the wall out to $y/\delta = 0.7$ with a -12% difference in the peak value.

The final profile point at $x_c = 1.381$ shows better agreement between the new model and the data in the outer region, but once again the trend of the data is not well followed. The k-ω model performs better than the other model in locating the position of the maximum shear stress. The error bounds mentioned for the previous profile point apply here as well. Thus, the k-ω model prediction falls relatively close to the experiment.

These results find the k-ω model superior to the new formulation at supersonic speeds, as well as to the k-ε model applied to this same data by Becht and Knight[16].

The inability of the present model to predict super-

sonic boundary layer behavior is expected, since adverse pressure gradients affect subsonic and supersonic boundary layers differently. Although the k-ω model performed well for Experiment (2), it is well known that none of the existing models perform well in regions of shock induced separation. As a result, a different diffusion model is necessary to improve existing predictions. This will require additional well documented experiments.

Concluding Remarks

The major contribution of the present work lies in the fact that it identifies inadequate diffusion modeling as the cause for the inability to model separated flows or flows on the verge of separation. The results suggest that a new diffusion mechanism needs to be introduced in the k - equation in order to explain observed behavior of turbulent flows in the presence of strong adverse pressure gradients at low speeds. The current modification of the k-ω model with an additional diffusion term based on the pressure gradient showed good agreement with a strong adverse pressure gradient in an incompressible flow. However, because subsonic and supersonic boundary layers behave differently in the presence of adverse pressure gradients, a more complete diffusion model is needed. This will require additional measurements and additional modeling.

Acknowledgments

The authors would like to express their sincere appreciation to Prof. Per-Age Krogstad for providing us with his digitized data and a copy of Dr. Per Egil Skare's Ph.D. dissertation. Computer resources were provided by the North Carolina Supercomputing Center.

References

1. Wilcox, D. C., *Turbulence Modeling in CFD*, DCW Industries, Inc., La Canada, CA, 1993.
2. Skare, P. E. and Krogstad, P. A., "A Turbulent Equilibrium Boundary Layer Near Separation", *Journal of Fluid Mechanics*, Vol. 272, August 1994, pp. 319-348.
3. Krogstad, P. A. and Skare, P. E., "Influence of a Strong Adverse Pressure Gradient on the Turbulent Structure in a Boundary Layer", *Physics of Fluids*, Vol. 7, no. 8, August 1995, pp. 2014-2024.
4. Bradshaw, P., "The Effect of Mean Compression or Dilatation on the Turbulence Structure of Supersonic Boundary Layers", *Journal of Fluid Mechanics*, Vol. 63, part 3, April 1974, pp. 449-464.
5. Fernando, E. M. and Smits, A. J., "A Supersonic Turbulent Boundary Layer in an Adverse Pressure Gradient", *Journal of Fluid Mechanics*, Vol. 211, 1990, pp. 285-307.
6. Stratford, B. S., "The Prediction of Separation of Turbulent Boundary Layers", *Journal of Fluid Mechanics*, Vol. 5, part 1, 1959, pp. 1-16.
7. Townsend, A. A., "Equilibrium Layers and Wall Turbulence", *Journal of Fluid Mechanics*, Vol. 11, part 1, August 1961, pp. 97-120.
8. Schubauer, G. B. and Klebanoff, P. S., "Investigation of Separation of the Turbulent Boundary Layer", NACA Report 1030, 1951
9. Saffman, P. G., "A Model for Inhomogeneous Turbulent Flow", *Proceedings of the Royal Society of London*, Vol. A317, 1970, pp. 417-433.
10. Harris, J. E. and Blanchard, D. K., "Computer Program for Solving Laminar, Transitional, or Turbulent Compressible Boundary Layer Equations for Two-Dimensional and Axisymmetric Flow", NASA TM 83207, February 1982.
11. Huang, P. G. and Bradshaw, P., "Law of the Wall for Turbulent Flows in Pressure Gradients", *AIAA Journal*, Vol. 33, no. 4, March 1995, pp. 624-632.
12. Bradshaw, P., "The Turbulence Structure of Equilibrium Boundary Layers", *Journal of Fluid Mechanics*, Vol. 29, part 4, September 1967, pp. 625-645.
13. Bradshaw, P. and Unsworth, K., Comment on "Evaluation of Preston Tube Calibration Equations in Supersonic Flow", *AIAA Journal*, Vol. 12, 1974, pp. 1293-1295.
14. Van Driest, E., "Turbulent Boundary Layer in Compressible Fluids", *Journal of Aerospace Science*, Vol. 18, 1951, pp. 145-160.
15. Carvin, C., Debieve, J., and Smits, A., "The Near Wall Temperature Profile of Turbulent Boundary Layers", *AIAA Paper* 88-0136, 1988.
16. Becht, R. and Knight, D., "A Simple Low Reynolds Number Modification for the Compressible k-ε Model Part I. Boundary Layer Flows", *AIAA Paper* 95-2218, 1995.

Figures

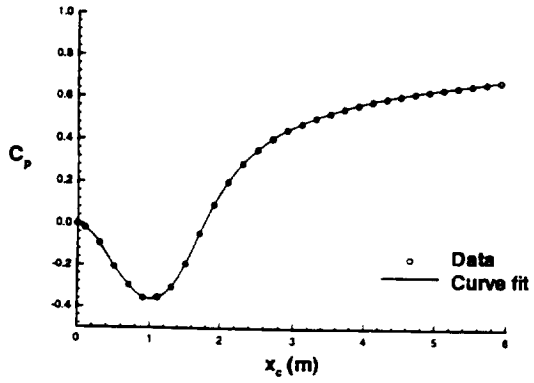

Figure 1. Pressure distribution and curve fit for Experiment (1).

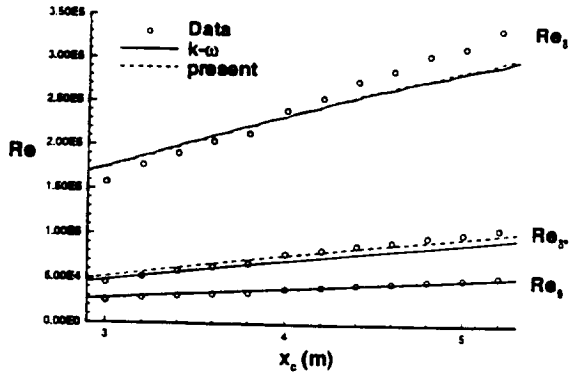

Figure 2. Comparison of length scale Reynolds numbers for Experiment (1).

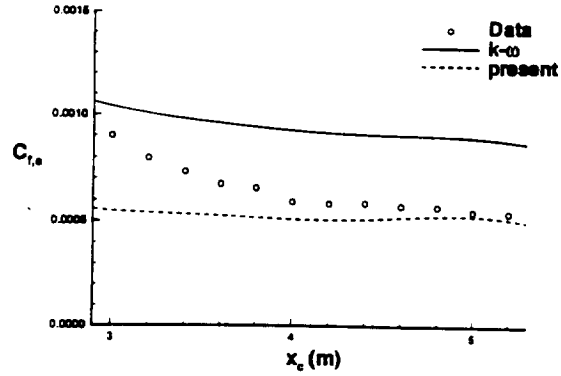

Figure 3. Comparison of skin friction for Experiment (1).

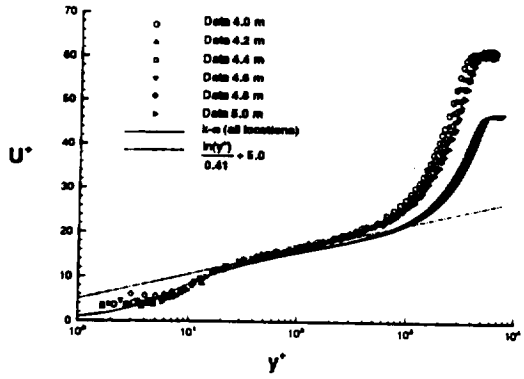

Figure 4. Comparison between k-ω model and data of the mean velocity profiles for Experiment (1).

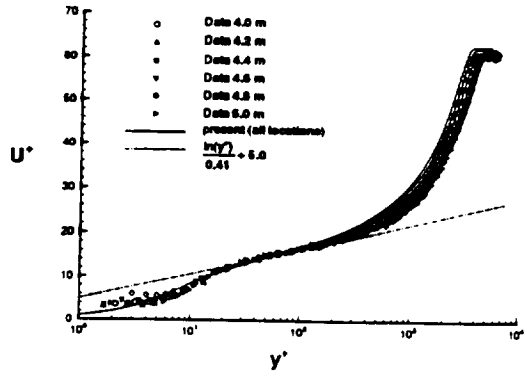

Figure 5. Comparison between present model and data of the mean velocity profiles for Experiment (1)

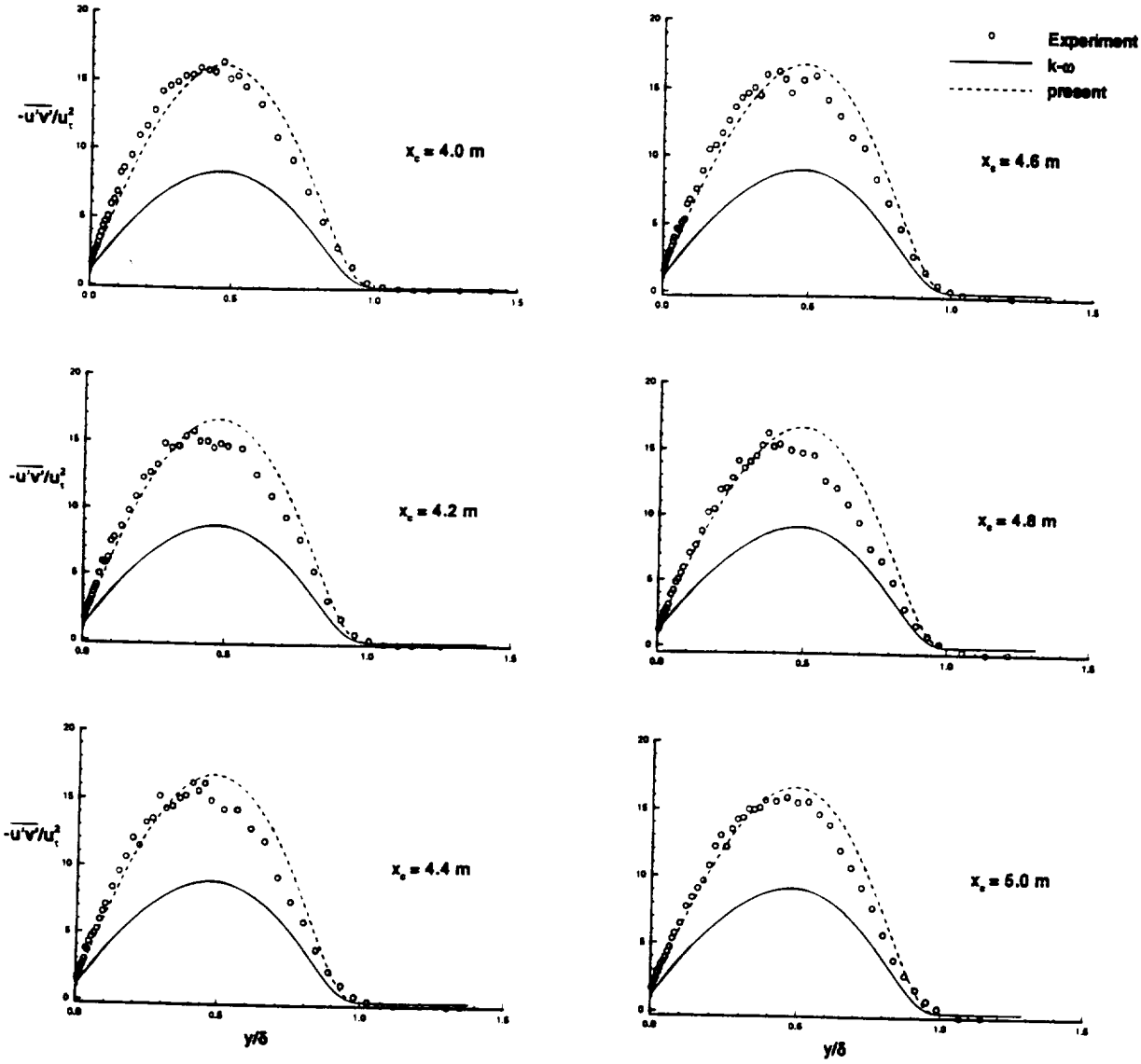

Figure 6. Comparison of shear stress profiles for Experiment (1).

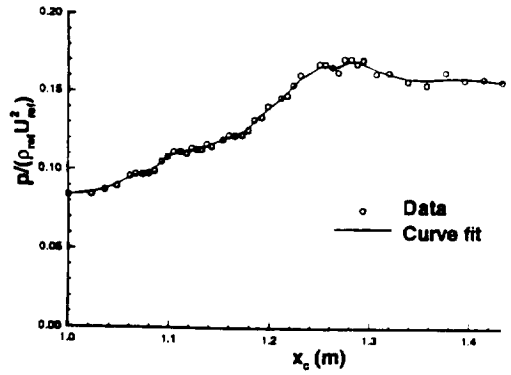

Figure 7. Pressure distribution and curve fit for Experiment (2).

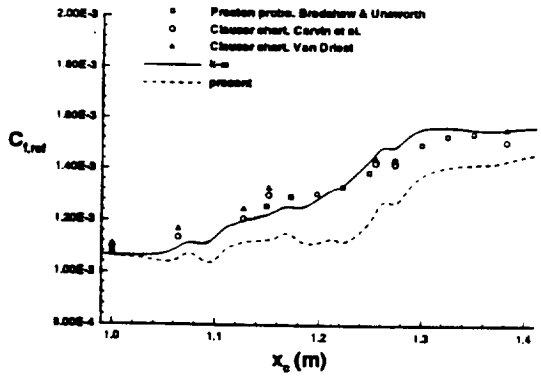

Figure 8. Comparison of skin friction values for Experiment (2).

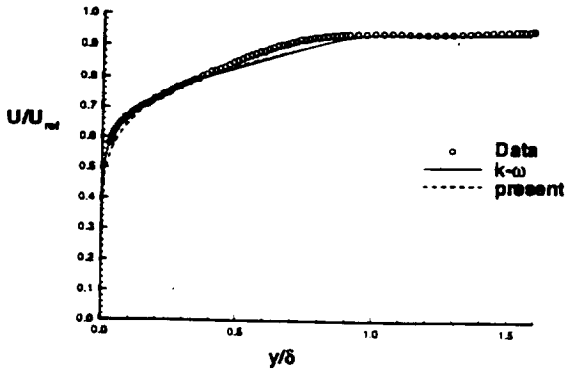

Figure 9. Comparison of mean velocity profile at x_c = 1.254 m for Experiment (2).

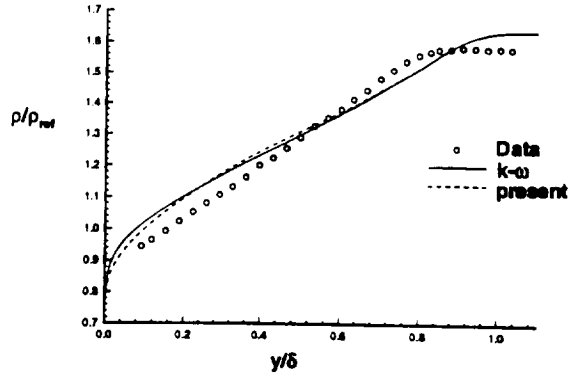

Figure 10. Comparison of mean density profile at x_c = 1.254 m for Experiment (2).

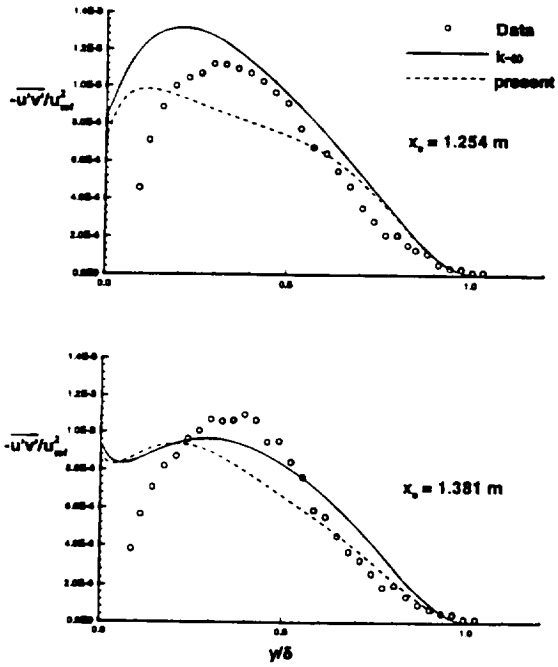

Figure 11. Comparison of shear stress profiles for Experiment (2).

AIAA 96-2039
A k - ζ (Enstrophy) Compressible Turbulence Model for Mixing Layers and Wall Bounded Flows

G. A. Alexopoulos
North Carolina State University
Raleigh, NC

H. A. Hassan
North Carolina State University
Raleigh, NC

27th AIAA Fluid Dynamics Conference
June 17-20, 1996 / New Orleans, LA

A k - ζ (ENSTROPHY) COMPRESSIBLE TURBULENCE MODEL FOR MIXING LAYERS AND WALL BOUNDED FLOWS

G. A. Alexopoulos *, and H. A. Hassan †
North Carolina State University, Raleigh, North Carolina 27695-7910

Abstract

A compressible turbulence model based on the k - ζ (enstrophy) model of Robinson et al. is developed to calculate free shear and wall bounded flows. The model is validated by comparing to the mixing layer data compiled by Settles and Dodson. It is shown that it reproduces measured similarity profiles of velocity, turbulent kinetic energy and shear stress. Moreover, its predictions are superior to the k - ϵ model with traditional compressibility corrections. Furthermore, the model predicts skin friction, heat transfer rates and law of the wall profiles with good accuracy for a variety of wall bounded flow cases.

Introduction

Currently, the two most used two-equation turbulence models are the k - ϵ and the k - ω models. Both of these models are not successful in predicting free shear flows and wall bounded flows with the same set of model constants and boundary conditions[1]. Part of the difficulty is a result of the fact that such models were originally derived for flows characterized by high turbulent Reynolds numbers. Although no adjustments are made in the traditional k - ω model at low turbulent Reynolds numbers[1], the adjustments made in the k - ϵ models are usually guided by asymptotic expansions and not by the exact form of the ϵ-equation. Because of this, it is believed that available low turbulent Reynolds number corrections employed in the k - ϵ model are not consistent with the exact ϵ-equation and thus lack the correct physics.

The above considerations were the basis of a new two-equation k - ζ (enstrophy) turbulence model developed by Robinson et al.[2] for incompressible flows. Instead of modeling the exact equation for dissipation, attention was focused on modeling the exact equation for the variance of vorticity, or enstrophy. Thus terms that depend on the mean flow, which are negligible at high turbulent Reynolds numbers but not a low turbulent Reynolds numbers, were retained and modeled. It is shown in Ref. [2] that the k - ζ model reproduces all available measurements of growth rates and turbulent shear stress distributions for a variety of free shear layers using the same set of model constants.

The objective of this work is to extended the k - ζ model of Robinson et al.[2] to compressible turbulent flows. The success of the k - ζ for reproducing a variety of incompressible flows should provide a good basis for the current model. As in the incompressible model, the current model will be based on the exact compressible equations to ensure that the correct physics is incorporated.

Compressible flows require for their description a velocity field and two thermodynamic variables such as the density and temperature. Because of this, the fluctuations of these thermodynamic variables are as important as those of the velocity in determining the resulting turbulent flow. As a result, traditional two-equation and stress models[3] have proven to be inadequate in describing such flows. Therefore, it appears that an appropriate compressible turbulent flow model of the "two-equation" variety, should include six equations that describe variances of velocity, density and temperature and their respective dissipation rates.

A simplification of the above approach can be achieved by invoking Morkovin's hypothesis[4]. According to this hypothesis, the pressure and total temperature fluctuations are small for non-hypersonic compressible boundary layers with conventional rates of heat transfer, i.e.

$$\frac{p'}{P} \ll 1 \quad , \quad \frac{T_o'}{T_o} \ll 1 \tag{1}$$

As a result,

$$\frac{\rho'}{\rho} \simeq -\frac{T'}{T} \simeq (\gamma - 1) M^2 \frac{u'}{U} \tag{2}$$

In the above equation, p', T_o', ρ', T' and u' are the fluctuating pressure, total temperature, density, temperature and velocity. Also M is the Mach number and γ is the ratio of specific heats. The remaining variables represent mean properties. Based on Eqn. (2), equations governing variances of turbulent quantities can be taken as the equation for the turbulent kinetic energy. However, equations governing the dissipation rates of the resulting variances may not be the same.

The approach employed in developing a k - ζ compressible model is to use the guidelines set in Ref. [2] to model

*Research Assistant, Mechanical and Aerospace Engineering, Student Member AIAA.

†Professor, Mechanical and Aerospace Engineering, Associate Fellow AIAA.

the additional terms. Thus, for low Mach numbers the new model reduces to that of Ref. [2]. It should be noted that existing k - ϵ models assume the effects of compressibility to be limited to the k-equation. This is not the case because the exact compressible ϵ-equation is different from that for incompressible flows.

Governing Equations

The mean-flow equations governing the conservation of mass, momentum and energy can be found in Ref. [1]. The compressible turbulent kinetic energy equation[1] (Favre-averaged) and enstrophy equation can be written as

$$\rho\frac{Dk}{Dt} = \tau_{ij}\frac{\partial\tilde{u}_i}{\partial x_j} - \rho\epsilon + \frac{\partial}{\partial x_j}\left(\overline{t_{ij}u_i''} - \overline{\rho u_j''\tfrac{1}{2}u_i''u_i''} - \overline{p'u_j''}\right) - \overline{u_i''}\frac{\partial P}{\partial x_i} + \overline{p'\frac{\partial u_i''}{\partial x_i}} \tag{3}$$

$$\begin{aligned}\rho\frac{D\zeta}{Dt} = {} & 2\rho\Big[\overline{\omega_i'\omega_j'}S_{ij} + \overline{\omega_i's_{ij}'}\Omega_j + \overline{\omega_i'\omega_j's_{ij}'} \\ & - \overline{\omega_i'^2}S_{jj} - \overline{\omega_i's_{jj}'}\Omega_i - \overline{\omega_i'^2 s_{jj}'} \\ & - \overline{\omega_i'u_j'}\frac{\partial\Omega_i}{\partial x_j} - \overline{u_j'\frac{\partial}{\partial x_j}(\omega_i'^2/2)}\Big] \\ & + \mu\frac{\partial^2\zeta}{\partial x_j\partial x_j} - 2\mu\overline{\frac{\partial\omega_i'}{\partial x_j}\frac{\partial\omega_i'}{\partial x_j}} \\ & - \frac{2\epsilon_{ijk}}{\rho}\left[\frac{\partial\rho}{\partial x_j}\overline{\omega_i'\frac{\partial t_{km}'}{\partial x_m}} - \left(\frac{\partial P}{\partial x_k} - \frac{\partial t_{km}}{\partial x_m}\right)\overline{\omega_i'\frac{\partial\rho'}{\partial x_j}}\right]\end{aligned} \tag{4}$$

where

$$\begin{aligned} S_{ij} &= \frac{1}{2}\left(\frac{\partial U_i}{\partial x_j} + \frac{\partial U_j}{\partial x_i}\right) & s_{ij}' &= \frac{1}{2}\left(\frac{\partial u_i'}{\partial x_j} + \frac{\partial u_j'}{\partial x_i}\right) \\ \Omega_i &= \epsilon_{ijk}\frac{\partial U_k}{\partial x_j} & \omega_i' &= \epsilon_{ijk}\frac{\partial u_k'}{\partial x_j} \\ k &= \tfrac{1}{2}\overline{u_i'u_i'} & \zeta &= \overline{\omega_i'\omega_i'} \\ \tau_{ij} &= -\overline{\rho u_i'u_j'} & \nu &= \frac{\mu}{\rho} \end{aligned} \tag{5}$$

$$t_{ij} = \mu\left(2S_{ij} - \frac{2}{3}\delta_{ij}S_{mm}\right)$$

Here ϵ is the turbulence energy dissipation rate, μ is the viscosity, Ω_i and ω_i' are the mean and fluctuating vorticity, t_{ij} and τ_{ij} are the laminar and turbulent (Reynolds) stress and ϵ_{ijk} is the permutation tensor.

The incompressible terms of Eqns. (3) and (4) were modeled in Ref. [2] with the remaining compressible terms modeled in the Appendices A and B. Upon modeling, Eqns. (3) and (4) take the form

$$\rho\frac{Dk}{Dt} = \tau_{ij}\frac{\partial U_i}{\partial x_j} + \frac{\partial}{\partial x_j}\left[\left(\frac{\mu}{3} + \frac{\mu_t}{\sigma_k}\right)\frac{\partial k}{\partial x_j}\right] - C_1\rho\frac{k}{\tau_\rho} - \mu\zeta \tag{6}$$

$$\begin{aligned}\rho\frac{D\zeta}{Dt} = {} & -\rho\frac{\partial\Omega_i}{\partial x_j}\left[\frac{1}{\sigma_r}\left(\frac{\partial\nu_t\Omega_i}{\partial x_j} + \frac{\partial\nu_t\Omega_j}{\partial x_i}\right)\right] \\ & - \rho\frac{\partial\Omega_i}{\partial x_j}\left[\epsilon_{mij}\left(\frac{\partial\left(\overline{u_m'u_l'}\right)}{\partial x_l} - \frac{\partial k}{\partial x_m}\right)\right] \\ & + \frac{\partial}{\partial x_j}\left[\left(\mu + \frac{\mu_t}{\sigma_\zeta}\right)\frac{\partial\zeta}{\partial x_j}\right] - \frac{\beta_5}{R_k}\rho\zeta^{\frac{3}{2}} \\ & + \left(\alpha_3\zeta b_{ij} + \frac{2}{3}\delta_{ij}\zeta\right)\rho S_{ij} - \frac{\beta_4\zeta\tau_{ij}\Omega_i\Omega_j}{k\Omega} \\ & + \epsilon_{ilm}\beta_8\left(\frac{\tau_{ij}}{k}\right)\frac{\partial k}{\partial x_l}\frac{\partial\zeta}{\partial x_m}\frac{\Omega_j}{\Omega^2} \\ & - \frac{2\beta_6\tau_{ij}\nu_t}{k\nu}\Omega\Omega_i\Omega_j + \frac{\beta_7\rho\zeta}{\Omega^2}\Omega_i\Omega_j S_{ij} \\ & - 2\rho\zeta S_{jj} - \frac{C_{\zeta_1}\rho\sqrt{2\zeta}}{\tau_\rho}\Omega - \frac{C_{\zeta_2}\rho}{\tau_\rho}\zeta \\ & - \frac{1}{\rho}\frac{\partial\rho}{\partial x_j}\left(\alpha_4\mu_t\frac{\partial\zeta}{\partial x_j} + \alpha_5\nu_t\zeta\frac{\partial\rho}{\partial x_j}\right) \\ & + \frac{2\alpha_8}{\rho\tau_\rho}\frac{\partial\rho}{\partial x_j}\left(\frac{\partial P}{\partial x_j} - \frac{\partial t_{ij}}{\partial x_i}\right)\end{aligned} \tag{7}$$

where

$$\tau_{ij} = \mu_t\left(2S_{ij} - \frac{2}{3}\delta_{ij}S_{mm}\right) - \frac{2}{3}\delta_{ij}\rho k \tag{8}$$

$$R_k = \frac{k}{\nu\sqrt{\zeta}} \quad , \quad \nu_t = \frac{\mu_t}{\rho}$$

with μ_t being the eddy (turbulent) viscosity.

Results and Discussion

To validate the present model, comparisons were made with various experimental measurements of compressible mixing layers and wall bounded flows. The model constants for the incompressible terms are tabulated in Ref. [2] and these were unchanged. The new terms are modeled in Appendices A and B. For the flows considered here, mixing layers and flat plates, only two terms were found to be significant. The first term appears in the k-equation (see Appendix A) and represents dilatational dissipation. The second term is in the ζ-equation (see Appendix B), $\overline{\omega_i's_{jj}'}\Omega_i$, which is a production term resulting from dilatational effects. The remaining terms, which may be important for other complex flows, are included for completeness. The model constants for the new compressible terms which were determined by numerical optimization are

$$C_1 = 0.6 \quad , \quad C_{\zeta_1} = 1.35$$

The ability of the model to calculate compressible mixing layers will be illustrated first. The two mixing layer cases that were chosen survived the scrutiny of Settles and

Dodson[5]. The first set is due to Samimy and Elliott[6] and Elliott and Samimy[7] while the second set is that of Goebel and Dutton[8]. Settles and Dodson tabulate and plot (see Table II and Fig. 1 of Ref. [5]) normalized mixing layer growth rates versus convective Mach numbers. The data is collected from various sources. As may be seen from the data and figure, there is a great deal of scatter rendering such tabulations and plots meaningless. The reason for the scatter can be traced to a lack of uniformity in calculating and defining growth rates. For most of the available data, the growth rate $db/dx \neq b/x$, where b is the width of the mixing layer. Moreover, there is a lack of uniformity in defining the width of the mixing layer. Because of this, judging the worth of a compressible turbulence theory based on its prediction of growth rates is somewhat misleading.

Rather than restrict our comparisons to growth rates, we opted to compare the predictions of the theory with the measured velocity, turbulent kinetic energy and turbulent shear stress. Since the k - ϵ model performs better than the k - ω model for free shear flows[1], comparisons were made with a k - ϵ model using the compressibility correction model proposed by Wilcox[1]. It may be recalled that this model incorporates the best feature of both Sarkar et al.[9] and Zeman's[10] models. Table 1 summarizes the cases given in Ref. [5] and described in Refs. [6] - [8].

Comparison of present theory with the k - ϵ model and experiment are shown in Figures 1 - 7. The computational procedure is similar to that employed in Ref. [2]. Taking compressibility into consideration, the similarity form of the variables for mixing layers is

$$\eta = \frac{\int \rho y\, dy}{\rho_1 x} \qquad u(x,y) = U_1 \mathcal{U}(\eta)$$

$$v(x,y) = \frac{\rho_1 U_1}{\rho}\left[\mathcal{V}(\eta) - \frac{\partial \eta}{\partial x} x \mathcal{U}(\eta)\right] \qquad h(x,y) = h_1 H(\eta)$$

$$k(x,y) = U_1^2 K(\eta) \qquad \zeta(x,y) = \frac{U_1^3}{\nu x} E(\eta)$$

$$\nu_t(x,y) = \left(\frac{\rho}{\rho_1}\right)^2 \frac{C_\mu U_1 x K^2(\eta)}{E(\eta)} \qquad N = C_\mu \frac{K^2(\eta)}{E(\eta)}$$

where the symbols have the same meaning as in Ref. [2].

In presenting the data, we followed the suggestion of Ref. [6] and scaled y with δ_w, the vorticity thickness, defined as

$$\delta_w = \frac{\Delta U}{\left(\frac{\partial u}{\partial y}\right)_{\max}} \quad , \quad \Delta U = U_1 - U_2 \tag{9}$$

where subscripts 1 and 2 represent the fast and slow streams, respectively. Each figure consists of three plots for normalized velocity, turbulent kinetic energy and turbulent shear stress, τ_{xy}.

It is seen from the figures that the present theory is in good agreement all cases of Refs. [6] and [7] and with cases 2, 3 and 4 of Ref [8]. For these cases, the k - ϵ model shows poor agreement with experiment. The agreement is not good with case 5 of Ref. [8], which is at the highest stagnation temperature ratio and convective Mach number. The reasons for this are not clear at this time. Note that this case is in good agreement with the k - ϵ model. Furthermore, applying the compressibility correction of Wilcox to the k - ζ model yields worse agreement with experiment than the k - ϵ with compressibility corrections.

To illustrate the ability of the model to compute more complex flows, three wall bounded flow cases were chosen and are summarized in Table 2. The first two cases are adiabatic wall cases obtained from the compressible turbulent boundary layer data compiled by Fernholz and Finley[11]. The first case is from from Shutts et al.[12] at $M_\infty = 2.24$ in air while the second set of data is that of Watson et al.[13] at $M_\infty = 10.31$ in helium. The third set of data is a cold wall case at $M_\infty = 8.18$ in air extracted from Kussoy and Horstman[14]. These cases were a subject of a previous investigation by Sommer et al.[15]

Calculation of the wall bounded flows was obtained using a marching boundary layer code, where the model boundary conditions are $k_\infty = k_w = \zeta_\infty = 0$ and $\frac{\partial \zeta}{\partial y}|_w = 0$. The eddy viscosity is defined as

$$\mu_t = C_\mu f_\mu \frac{\rho k^2}{\nu \zeta} \quad , \quad C_\mu = 0.09 \tag{10}$$

where

$$f_\mu = \min(f_\mu^*, 1.0)$$

$$f_\mu^* = \left(1 + \frac{C_{\mu_1}}{\sqrt{Re_t}}\right) \tanh\left(\frac{y^+}{C_{\mu_2}}\right) \tag{11}$$

and

$$y^+ = \frac{y u_\tau}{\nu} \ , \ u_\tau = \sqrt{\frac{\tau_w}{\rho}} \ , \ C_{\mu_1} = 0.5 \ , \ C_{\mu_2} = 29.5 \tag{12}$$

Comparisons of the k - ζ model with the experiment are shown in Figures 8 - 10. In presenting the results, we followed the suggestions in the critical review of the data by Fernholz and Finley[16]. It was determined in the review that certain differences were observed in the data that were due to a sensitivity to the plotting method rather that from an observed physical phenomenon. Furthermore, it was suggested that a plot of T/T_δ versus U/U_δ represents a valid comparison for temperature for examining the Crocco - van Driest relation. The first two experimental cases use the Crocco - van Driest relation by assuming constant total enthalpy and pressure across the boundary layer to determine the temperature profiles from the measured velocity profiles. As a consequence, the temperature data is not an independent measurement for these two cases.

Each figure consists of a plot of temperature versus velocity distribution and a law of the wall comparison between the experiment and present theory. The calculations for each case were performed by matching the respective experimental Re_θ, given in Table 2. It can be

seen from Figures 8 and 9 that the k - ζ model predicts the experiment with good accuracy. However, there is a slight discrepancy between theory and experiment for the law of the wall distribution of Figure 9. It was determined in Ref. [16] that this case may not have been fully turbulent, which may explain the differences in the law of the wall. The difference in measured C_f (given in Table 2) and theory for these two adiabatic wall cases is 0.1% and 1.5%, respectively.

In Ref. [14] the measurements of velocity and temperature are obtained independently. Figure 10 represents the cold wall case comparisons and is showing an excellent agreement between experiment and present theory. Further, the difference in measured C_f and C_h for this case is 5.6% and 8.6%, respectively, which is well within experimental error.

Conclusions

Comparison between experiment and theory show good agreement in the calculation of compressible mixing layers. Furthermore, the current k - ζ was shown to be generally superior to k - ϵ model in predicting mixing layer experiments. Finally, an examination of compressible wall bounded flows show an excellent agreement in the calculation of skin friction and heat transfer rates and a good prediction of temperature profiles and law of the wall distribution. Future work will involve further validation by implementing the model in a Navier-Stokes solver and calculating more complex flows.

Acknowledgments

This work is supported in part by NASA Grant NAG-1-244. The authors would like to acknowledge many helpful discussions with Prof. Craig Dutton of the University of Illinois at Urbana-Champaign and Prof. Mo Samimy of the Ohio State University. Part of the computations were carried out at the North Carolina Supercomputing Center.

References

[1] Wilcox, D. C. *"Turbulence Modeling for CFD"*. DCW Industries, Inc., La Canada, CA, 1993.

[2] Robinson, D. F., Harris, J. E., and Hassan, H. A. "Unified Turbulence Closure Model for Axisymmetric and Planar Free Shear Flows". *AIAA Journal*, Vol. 33(No. 12):pp. 2325–2331, December 1995.

[3] Speziale, C. G., Abid, R., and Mansour, N. N. "Evaluation of Reynolds Sress Turbulence Closures in Compressible Homogeneous Shear Flow". ICASE Report 94-17, March 1994.

[4] Morkovin, M. "Effects of Compressibility on Turbulent Flows". In *"Mecanique de la Turbulence"*. CNRS, A. Favre, editor, pp. 367-380, Gordon and Breach, 1964.

[5] Settles, G. S., and Dodson, L. J. "Hypersonic Turbulent Boundary-Layer and Free Shear Database". NASA CR 177610, April 1993.

[6] Samimy, M., and Elliott, G. S. "Effects of Compressibility on Characteristics of Free Shear Layers". *AIAA Journal*, Vol. 28(No. 3):pp. 439–445, March 1990.

[7] Elliott, G. S., and Samimy, M. "Compressibility Effects in Free Shear Layers". *Physics of Fluids A*, Vol. 2(No. 7):pp. 1231–1240, July 1990.

[8] Goebel, S. G., and Dutton, J. C. "Experimental Study of Compressible Turbulent Mixing Layers". *AIAA Journal*, Vol. 29(No. 4):pp. 538–546, April 1991.

[9] Sarkar, S., Erlebacher, G., Hussaini, M.Y ., and Kreiss, O. "The Analysis and Modeling of Dilatational Terms in Compressible turbulence". *Journal of Fluid Mechanics*, Vol. 227:pp. 473–493, June 1991.

[10] Zeman, O. "Dilatational Dissipation: The Concept and Application in Modeling Compressible Mixing Layers". *Physics of Fluids A*, Vol. 2(No. 2):pp. 178–188, February 1990.

[11] Fernholz, H. H., and Finley, P. J. "A Critical Compilation of Compressible Turbulent Boundary Layer Data". AGARDograph No. 223, June 1977.

[12] Shutts, W. H., Hartwig, W. H., and Weiler, J. E. "Final Report on Turbulent Boundary Layer and Skin Friction Measurements on a Smooth Thermally Insulated Flat Plate at Supersonic Speeds". Report No. DRL-365 CM-823, 1955.

[13] Watson, R. D., Harris, J. E., and Anders, J. B. "Measurements in a Transitional/Turbulent Mach 10 Boundary Layer at High-Reynolds Numbers". AIAA Paper 73-165, January 1973.

[14] Kussoy, M. I., and Horstman, K. C. "Documentation of Two- and Three-Dimensional Shock-Wave/Turbulent-Boundary-Layer Interaction Flows at Mach 8.2". NASA TM 103838, May 1991.

[15] Sommer, T. P., So, R. M. C., and Zhang, H. S. "Supersonic Flow Calculation Using a Reynolds-Stress and an Eddy Thermal Diffusivity Turbulence Model". NASA CR 4515, June 1993.

[16] Fernholz, H. H., and Finley, P. J. "A Critical Commentary on Mean Flow Data for Two-Dimensional Compressible Turbulent Boundary Layers". AGARDograph No. 253, May 1980.

[17] Ristorcelli, J. R. "A Pseudo-Sound Constitutive Relationship for the Dilatational Covariances in Compressible Turbulence: An Analytical Theory ". ICASE Report 95-22, March 1995.

Appendix A: Modeling of the k Equation

The dissipation rate in Eqn. (3) is defined as

$$\rho\epsilon = \nu\left[\overline{\rho\omega_i''\omega_i''} + 2\overline{\rho u_{i,j}'' u_{j,i}''} - \frac{2}{3}\overline{\rho u_{i,i}'' u_{i,i}''}\right] \quad \text{(A.1)}$$

$$= \nu\left[\overline{\rho\omega_i''^2} + \frac{4}{3}\overline{\rho\left(u_{i,i}''\right)^2}\right] + 2\nu\frac{\partial}{\partial x_i}\left[\frac{\partial}{\partial x_j}\left(\overline{\rho u_i'' u_j''}\right) - 2\overline{\rho u_i''\frac{\partial u_j''}{\partial x_j}}\right] \quad \text{(A.2)}$$

The second term in Eq. (A.2) can be written as

$$2\nu\frac{\partial}{\partial x_i}\left[\frac{\partial}{\partial x_j}\left(\overline{\rho u_i'' u_j''}\right) - 2\overline{\rho u_i''\frac{\partial u_j''}{\partial x_j}}\right]$$

$$\simeq 2\frac{\partial}{\partial x_i}\left[\nu\left\{\frac{\partial}{\partial x_j}\left(\overline{\rho u_i'' u_j''}\right) - 2\overline{\rho u_i''\frac{\partial u_j''}{\partial x_j}}\right\}\right] \quad \text{(A.3)}$$

and is normally neglected, consistent with the assumptions of homogeneous turbulence. In this work, the term is included in the diffusion term.

The approach employed in modeling the various terms follows closely that employed in Ref. [2]. Moreover, model constants developed in Ref. [2] were unchanged in this model.

The compressibility term in the k equation has generated a great deal of discussion lately and led to the developments of models by Sarkar et al.[9], Zeman[10], Wilcox[1] and Ristorcelli[17] among others. None of these models were adopted here because they do not blend smoothly with the incompressible limit. Moreover, there is no reason to assume that the time scale governing this term is dependent on ζ. Instead the term

$$\nu\frac{4}{3}\overline{\rho\left(u_{i,i}''\right)^2} \quad \text{(A.4)}$$

is modeled as

$$C_1\frac{k}{\tau_\rho} \quad \text{(A.5)}$$

where C_1 is a model constant and τ_ρ is a time scale. Because the term under consideration is zero when the density is constant, τ_ρ is modeled as

$$\frac{1}{\tau_\rho} = \frac{1}{\rho}\sqrt{\left(\frac{\partial\rho}{\partial x_j}\right)^2 k} \quad \text{(A.6)}$$

Appendix B: Modeling of the ζ Equation

1. $\overline{\omega_i' s_{jj}'}$

The above first order tensor quantity has units of $\left[\frac{1}{s^2}\right]$ and is modeled as

$$\overline{\omega_i' s_{jj}'} = \overline{\omega_i'\frac{\partial u_j'}{\partial x_j}} = C_{\zeta_1}\frac{\sqrt{2\zeta}}{\tau_\rho\Omega}\Omega_i \quad \text{(B.1)}$$

where $1/\tau_\rho$ was defined in Appendix A and $\Omega = \sqrt{\Omega_i\Omega_i} = |\Omega_i|$.

2. $\overline{\omega_i'^2 s_{jj}'}$

The above scalar quantity has units of $\left[\frac{1}{s^3}\right]$ and is modeled as

$$\overline{\omega_i'^2 s_{jj}'} = \overline{\omega_i'^2\frac{\partial u_j'}{\partial x_j}} = C_{\zeta_2}\frac{\zeta}{2\tau_\rho} \quad \text{(B.2)}$$

3. $\epsilon_{ijk}\overline{\omega_i'\frac{\partial t_{km}'}{\partial x_m}}$

The quantity t_{km}' is defined as

$$t_{km}' = \mu\left(\frac{\partial u_k'}{\partial x_m} + \frac{\partial u_m'}{\partial x_k}\right) + \lambda\delta_{km}\frac{\partial u_j'}{\partial x_j} \quad \text{(B.3)}$$

where $\lambda = -\frac{2}{3}\mu$. Thus,

$$\frac{\partial t_{km}'}{\partial x_m} = \mu\left(\frac{\partial^2 u_k'}{\partial x_m^2} + \frac{\partial^2 u_m'}{\partial x_k x_m}\right) + \lambda\delta_{km}\frac{\partial^2 u_j'}{\partial x_m x_j} \quad \text{(B.4)}$$

$$= \mu\left(\frac{\partial^2 u_k'}{\partial x_m^2} + \frac{\partial^2 u_m'}{\partial x_k x_m}\right) + \lambda\frac{\partial^2 u_j'}{\partial x_k x_j} \quad \text{(B.5)}$$

$$= \mu\frac{\partial^2 u_k'}{\partial x_m^2} + (\lambda+\mu)\frac{\partial^2 u_j'}{\partial x_k x_j} \quad \text{(B.6)}$$

and

$$\epsilon_{ijk}\overline{\omega_i'\frac{\partial t_{km}'}{\partial x_m}} = \overline{\mu\epsilon_{ijk}\omega_i'\frac{\partial^2 u_k'}{\partial x_m^2}} + \overline{(\lambda+\mu)\epsilon_{ijk}\omega_i'\frac{\partial^2 u_j'}{\partial x_k x_j}} \quad \text{(B.7)}$$

$$= \overline{2\mu r_{kj}'\frac{\partial^2 u_k'}{\partial x_m^2}} + \overline{2(\lambda+\mu)r_{kj}'\frac{\partial^2 u_j'}{\partial x_k x_j}} \quad \text{(B.8)}$$

where $2r'_{kj} = \epsilon_{ijk}\omega'_i$. Using the gradient diffusion approximation, the above terms can be modeled as

$$\overline{2\mu r'_{kj}\frac{\partial^2 u'_k}{\partial x_m^2}} = \alpha_4\frac{\mu_t}{2}\frac{\partial\zeta}{\partial x_j} \qquad \text{(B.9)}$$

$$\overline{2(\lambda+\mu)r'_{kj}\frac{\partial^2 u'_j}{\partial x_k x_j}} = \alpha_5\frac{\zeta\nu_t}{2}\frac{\partial\rho}{\partial x_j} \qquad \text{(B.10)}$$

Hence, the term in question is modeled as

$$\epsilon_{ijk}\overline{\omega'_i\frac{\partial t'_{km}}{\partial x_m}} = \alpha_4\frac{\mu_t}{2}\frac{\partial\zeta}{\partial x_j} + \alpha_5\frac{\zeta\nu_t}{2}\frac{\partial\rho}{\partial x_j} \qquad \text{(B.11)}$$

4. $\epsilon_{ijk}\overline{\omega'_i\frac{\partial\rho'}{\partial x_j}}$

Since

$$\epsilon_{ijk}\overline{\omega'_i\frac{\partial\rho'}{\partial x_j}} = -2\overline{r'_{jk}\frac{\partial\rho'}{\partial x_j}} \qquad \text{(B.12)}$$

is a vector, it is modeled as

$$\epsilon_{ijk}\overline{\omega'_i\frac{\partial\rho'}{\partial x_j}} = \frac{\alpha_8}{\tau_\rho}\frac{\partial\rho}{\partial x_k} \qquad \text{(B.13)}$$

Table 1: Mixing Layer Experiments

Case	U_2/U_1	ρ_2/ρ_1	T_{o_1}/T_{o_2}	T_{o_1}, T_{o_2} (K)	M_1, M_2	M_c
Samimy and Elliott - Case 1	0.36	0.64	1.00	276, 276	1.80, 0.51	0.51
Samimy and Elliott - Case 2	0.25	0.58	1.00	276, 276	1.96, 0.37	0.64
Elliott and Samimy - Case 3	0.25	0.37	1.00	276, 276	3.03, 0.45	0.86
Goebel and Dutton - Case 2	0.57	1.55	1.96	578, 295	1.91, 1.36	0.46
Goebel and Dutton - Case 3	0.18	0.57	1.00	285, 285	1.96, 0.27	0.69
Goebel and Dutton - Case 4	0.16	0.60	1.24	360, 290	2.35, 0.30	0.86
Goebel and Dutton - Case 5	0.16	1.14	2.25	675, 300	2.27, 0.38	0.99

$M_c = (U_1 - U_c)/a_1 \quad , \quad U_c = (a_1U_2 + a_2U_1)/(a_1 + a_2)$

Table 2: Wall Bounded Experiments

Case	M_∞	P_{o_∞} (MPa)	T_{o_∞} (K)	Re_θ	T_w/T_{aw}	C_fx10^{-3}	C_hx10^{-3}
Shutts et al.	2.24	0.2364	339	20797	1.0	1.62	0
Watson et al.	10.31	7.5576	300	15074	1.0	0.24	0
Kussoy and Horstman	8.18	6.0795	1166	4600	0.3	0.98	0.53

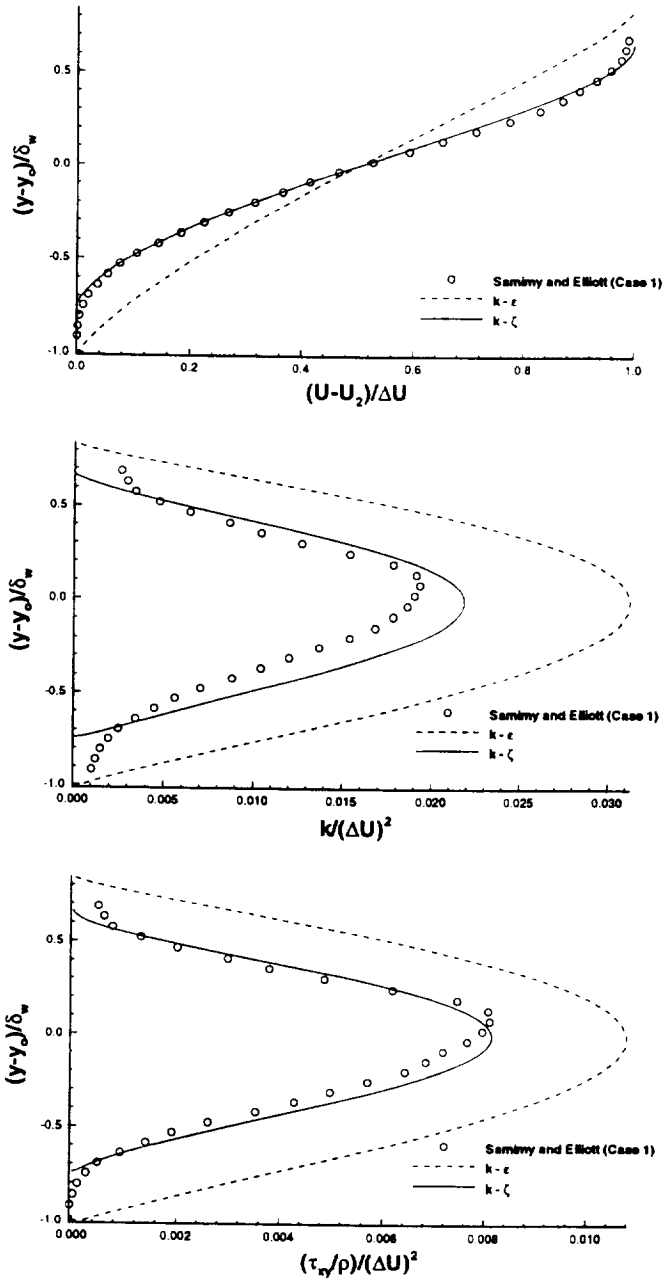

Figure 1: Turbulence Model Comparisons with Experiment (Samimy and Elliott Case 1)

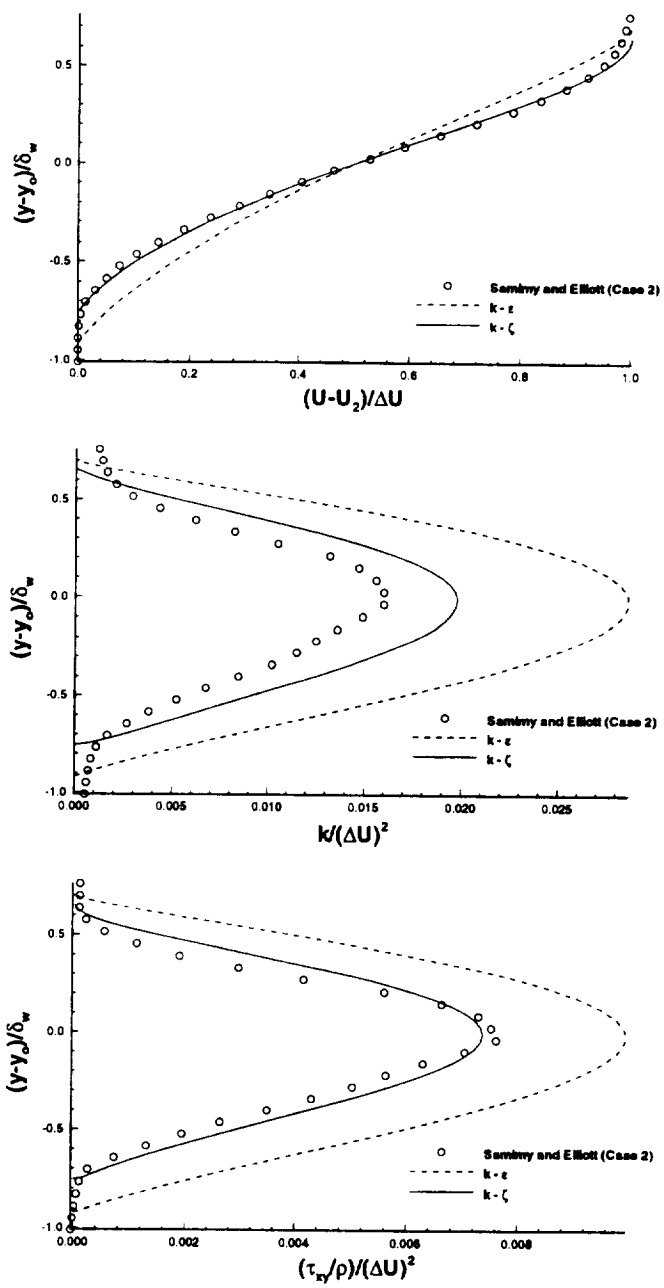

Figure 2: Turbulence Model Comparisons with Experiment (Samimy and Elliott Case 2)

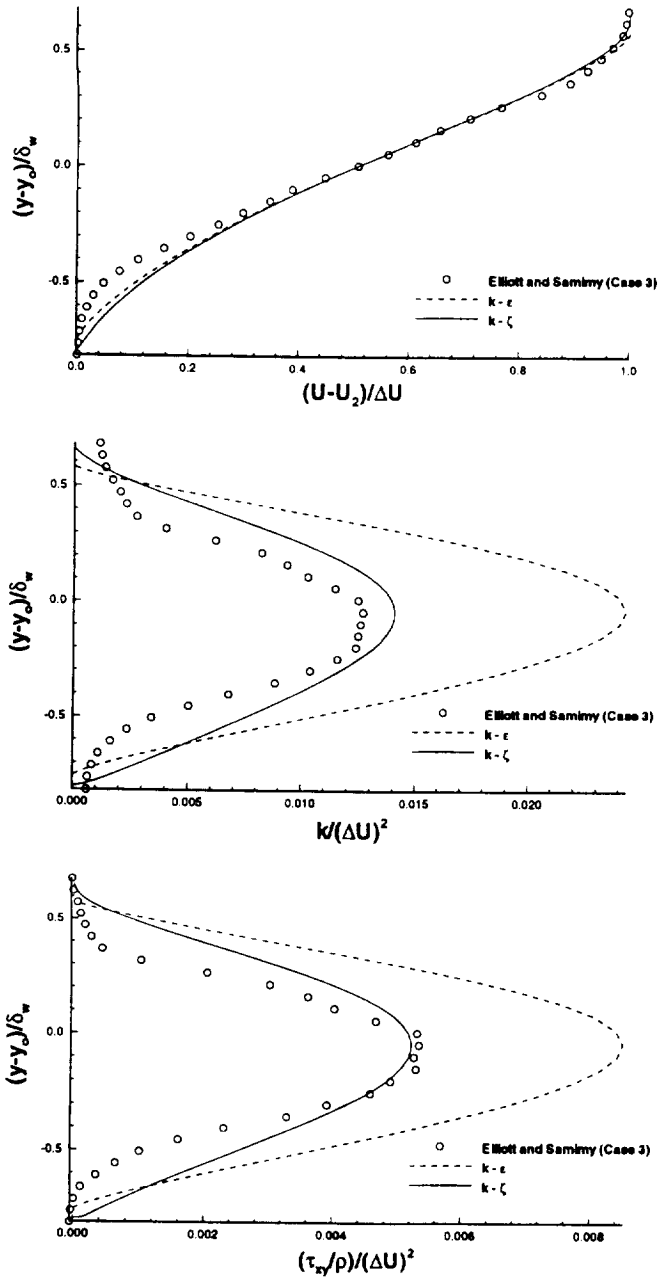

Figure 3: Turbulence Model Comparisons with Experiment (Elliott and Samimy Case 3)

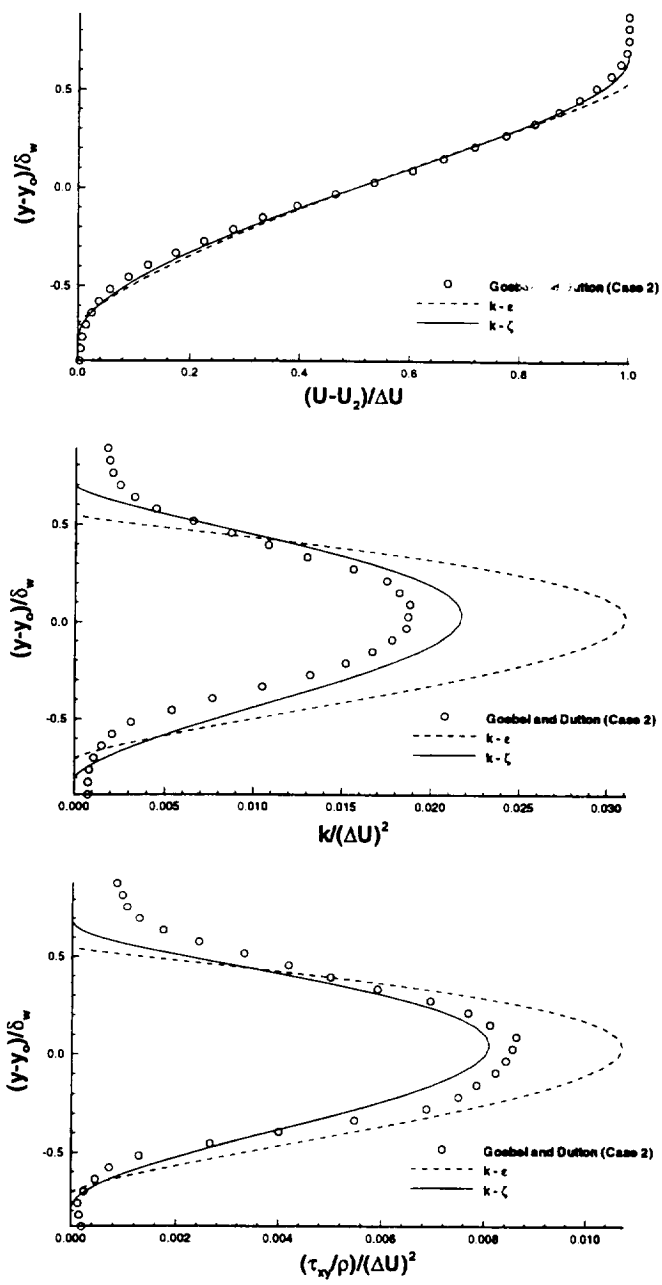

Figure 4: Turbulence Model Comparisons with Experiment (Goebel and Dutton Case 2)

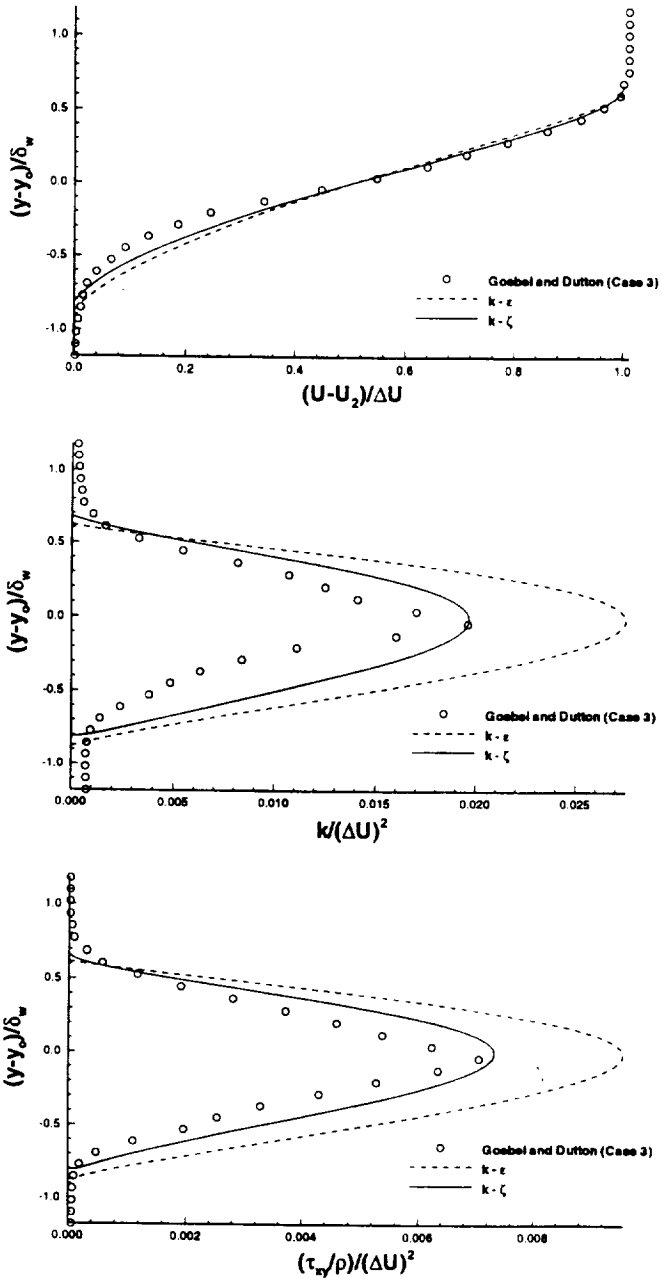

Figure 5: Turbulence Model Comparisons with Experiment (Goebel and Dutton Case 3)

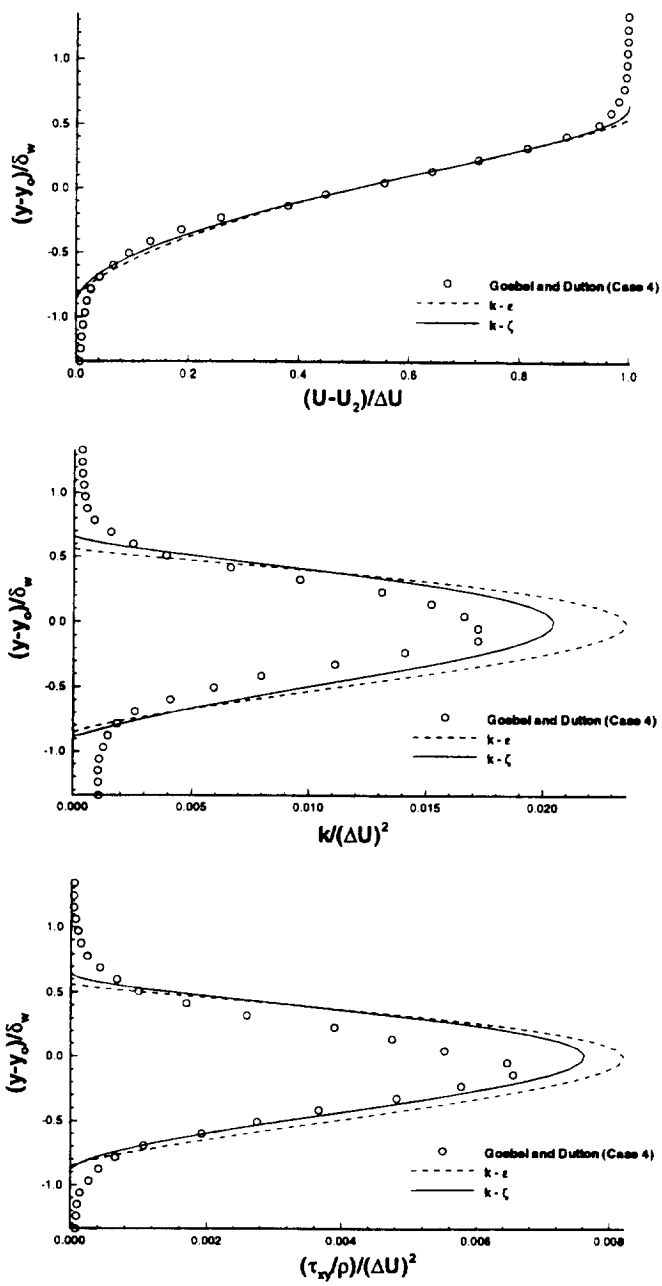

Figure 6: Turbulence Model Comparisons with Experiment (Goebel and Dutton Case 4)

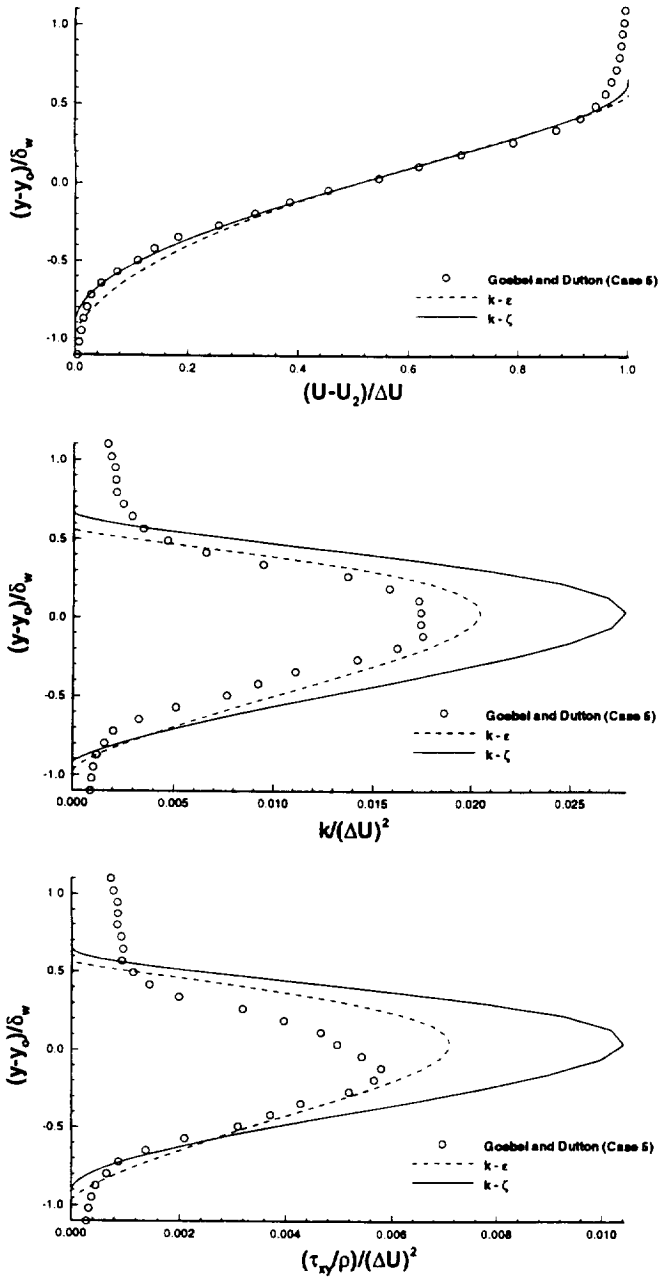

Figure 7: Turbulence Model Comparisons with Experiment (Goebel and Dutton Case 5)

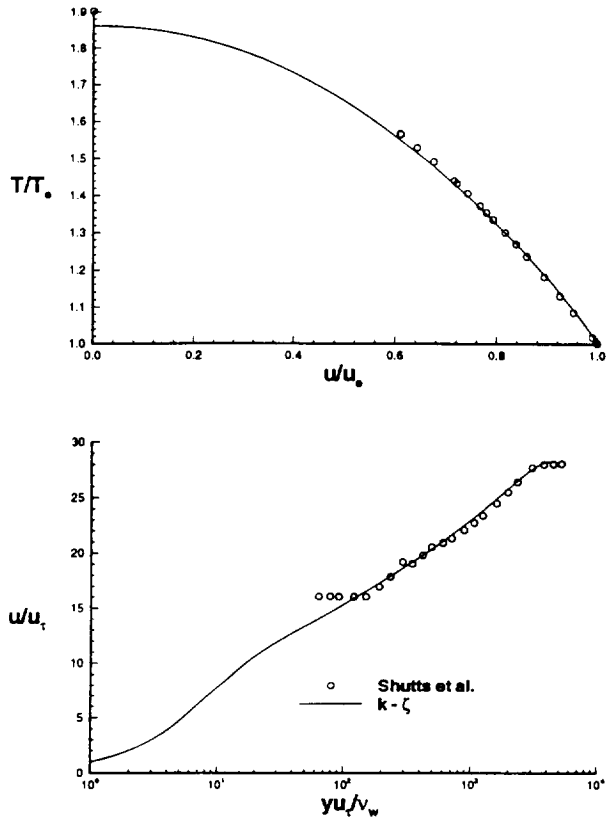

Figure 8: Comparison of Calculated Mean Temperature - Velocity Distribution and Law of the Wall versus Experiment (Shutts et al.)

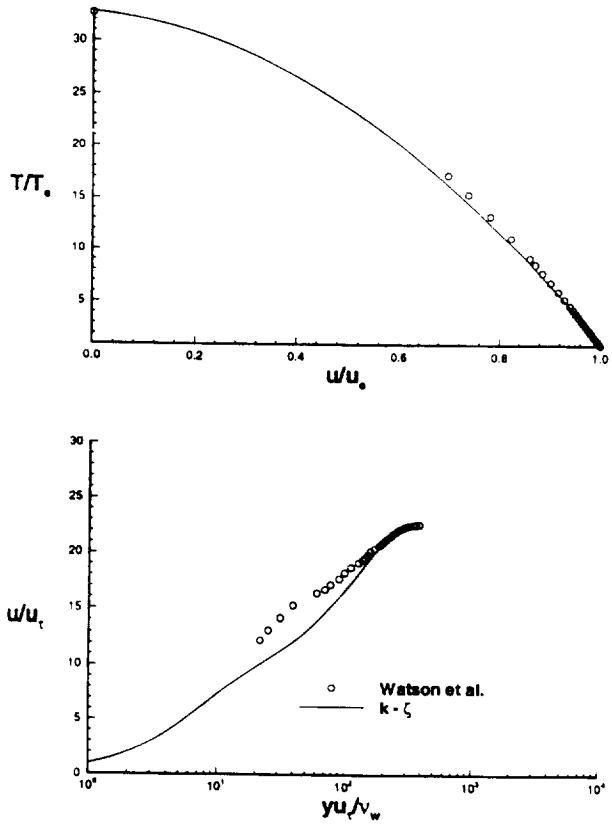

Figure 9: Comparison of Calculated Mean Temperature - Velocity Distribution and Law of the Wall versus Experiment (Watson et al.)

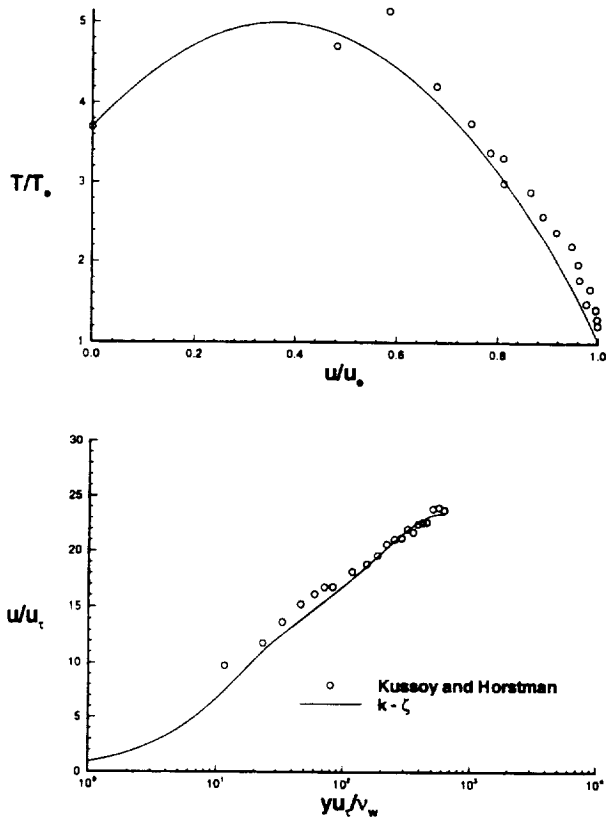

Figure 10: Comparison of Calculated Mean Temperature - Velocity Distribution and Law of the Wall versus Experiment (Kussoy and Horstman)

AIAA 96-2057
A Two-Equation Turbulence Closure Model for Wall Bounded and Free Shear Flows

David F. Robinson
North Carolina State University
Raleigh, NC

H.A. Hassan
North Carolina State University
Raleigh, NC

27th AIAA Fluid Dynamics Conference
June 17-20, 1996 / New Orleans, LA

A Two-Equation Turbulence Closure Model for Wall Bounded and Free Shear Flows

David F. Robinson *
North Carolina State University, Raleigh, North Carolina 27695-7910

H. A. Hassan †
North Carolina State University, Raleigh, North Carolina 27695-7910

Abstract

The two-equation turbulence model of Robinson et al. is examined for a variety of wall bounded cases including a boundary layer solution of a flat plate and a Navier-Stokes solution of airfoils. It is shown that traditional methods of modeling turbulent diffusion are not appropriate for describing turbulent separated flows. A tentative proposal for modeling such flows is presented and the predictions of the model are compared with measurements for a difficult case involving an NACA 0012 airfoil. The results presented here clearly illustrate that a two-equation turbulence model can be developed to describe a variety of flows, for which a two-equation model is appropriate, using the same set of model constants.

Introduction

Existing k-ω and k-ϵ turbulence closure models are incapable of describing wall bounded and free shear flows using the same set of model constants and boundary conditions. It is generally agreed that the problem with existing models comes from the dissipation equation, ϵ or ω. The reason for this can be traced to the fact that these equations were developed for high turbulent Reynolds numbers, Re_t, but are being employed in situations where Re_t is low.

For most turbulent shear flows Re_t is typically large enough so that one can assume the small scales are nearly independent of the large scales and thus their dissipation rate is isotropic. If one makes this isotropic assumption then the terms in the exact dissipation equation which depend on the mean flow can be neglected. However, for most shear flows, the turbulent Reynolds number varies from very large values in the bulk of the flow to very small values near walls and outside of the boundary layer.

For regions of low Re_t, the small scales of turbulence are weakly dependent on the large scales, and therefore, on the mean flow. Because of this, terms appearing in the exact dissipation equation which depend on the mean flow cannot be neglected.

The above considerations were the basis of a new two-equation model [1]. Instead of modeling the exact equation for dissipation, attention was focused on the enstrophy or the variance of vorticity equation [2]. The model developed in Ref. [1] was used to describe free shear layers (wakes, jets, and mixing layers). The same set of model constants was used in all calculations. Excellent predictions of growth rates, shear stress, and velocity distributions were obtained. The object of this work is to use the same set of model constants developed in Ref. [1] to study wall bounded flows. The implementation of the model will proceed in a number of stages. In the first, the model is implemented in a boundary layer code [3] and the results are illustrated by calculating a flow past a flat plate and its wake. Second, the model is implemented in a Navier-Stokes code [4] and the results are illustrated by calculating attached flows past airfoils. In the third, attention was devoted to separated flows past airfoils. It was determined that traditional models of turbulent diffusion are not adequate for calculating separated flows. This resulted in the development of a tentative diffusion model.

The model was validated by calculating flows past an NACA 0012 at an angle of attack, α, of 2.26 deg and a free stream Mach number, M_∞, of 0.79. It may be recalled [5] that existing two-equation models were unable to predict the pressure distribution for this case; only the Johnson and King model [6] performed well for this case. The results presented are intended to demonstrate that one set of model constants can be used to describe all types of shear flows. Obviously, applications were limited to those cases where a two-equation model is expected to give good results.

*Research Assistant, Mechanical and Aerospace Engineering, Student Member AIAA.

†Professor, Mechanical and Aerospace Engineering, Associate Fellow AIAA.

Analysis

Assuming incompressible flow, the governing equations are the Reynolds averaged continuity, momentum, turbulent kinetic energy, and enstrophy. These equations can be written as

$$\frac{\partial U_i}{\partial x_i} = 0 \tag{1}$$

$$\frac{DU_i}{Dt} = -\frac{1}{\rho}\frac{\partial P}{\partial x_i} + \frac{\partial}{\partial x_j}\left(2\nu S_{ij} - \overline{u_i' u_j'}\right) \tag{2}$$

$$\begin{aligned}\frac{Dk}{Dt} &= \frac{\tau_{im}}{\rho}\frac{\partial U_i}{\partial x_m} - \nu\zeta \\ &- \frac{\partial}{\partial x_m}\left[\frac{\overline{u_i' u_i' u_m'}}{2} + \frac{\overline{p' u_m'}}{\rho} - \nu\epsilon_{ikm}\frac{\partial(\overline{u_i'\omega_m'})}{\partial x_k}\right]\end{aligned} \tag{3}$$

$$\begin{aligned}\frac{D\zeta}{Dt} &= -2\overline{u_j'\omega_i'}\frac{\partial\Omega_i}{\partial x_j} - \frac{\partial\left(\overline{u_j'\omega_i'\omega_i'}\right)}{\partial x_j} + 2\overline{\omega_i'\omega_j' s_{ij}'} \\ &+ 2\overline{\omega_i'\omega_j'}S_{ij} + 2\overline{\omega_i' s_{ij}'}\Omega_j + \nu\frac{\partial^2\zeta}{\partial x_j\partial x_j} \\ &- 2\nu\overline{\frac{\partial\omega_i'}{\partial x_j}\frac{\partial\omega_i'}{\partial x_j}}\end{aligned} \tag{4}$$

where,

$$\begin{aligned} s_{ij}' &= \frac{1}{2}\left(\frac{\partial u_i'}{\partial x_j} + \frac{\partial u_j'}{\partial x_i}\right) & S_{ij} &= \frac{1}{2}\left(\frac{\partial U_i}{\partial x_j} + \frac{\partial U_j}{\partial x_i}\right) \\ \Omega_i &= \epsilon_{ijk}\frac{\partial U_k}{\partial x_j} & \omega_i' &= \epsilon_{ijk}\frac{\partial u_k'}{\partial x_j} \\ k &= \frac{\overline{u_i' u_i'}}{2} & \zeta &= \overline{\omega_i'\omega_i'} \\ \tau_{ij} &= -\rho\overline{u_i' u_j'} & \nu &= \frac{\mu}{\rho} \end{aligned} \tag{5}$$

ρ is the density, μ is the viscosity, u_i', ω_i', and p' are the fluctuating velocity, vorticity, and pressure, and U_i is the mean velocity. Equations 3 and 4 were modeled in Ref. [1] and the results can be written as

$$\rho\frac{Dk}{Dt} = \tau_{im}\frac{\partial U_i}{\partial x_m} - \mu\zeta + \frac{\partial}{\partial x_m}\left[\left(\frac{\mu}{3} + \frac{\mu_t}{\sigma_k}\right)\frac{\partial k}{\partial x_m}\right] \tag{6}$$

$$\begin{aligned}\frac{D\zeta}{Dt} &= -\frac{\partial\Omega_i}{\partial x_j}\left(\frac{\nu_t}{\sigma_r}\left[\frac{\partial\Omega_i}{\partial x_j} + \frac{\partial\Omega_j}{\partial x_i}\right]\right) \\ &-\frac{\partial\Omega_i}{\partial x_j}\left(\epsilon_{mij}\left[\frac{\partial\left(\overline{u_m' u_l'}\right)}{\partial x_l} - \frac{\partial k}{\partial x_m}\right]\right) \\ &+\frac{\partial}{\partial x_j}\left[\left(\nu + \frac{\nu_t}{\sigma_\zeta}\right)\frac{\partial\zeta}{\partial x_j}\right] - \frac{\beta_5}{R_k}\zeta^{\frac{3}{2}} \\ &+\left(\alpha_3\zeta b_{ij} + \frac{2}{3}\delta_{ij}\zeta\right)S_{ij} - \frac{\beta_4\zeta\tau_{ij}\Omega_i\Omega_j}{\rho k\Omega} \\ &+2\beta_8\epsilon_{ilm}\left(\frac{\tau_{ij}}{\rho k}\right)\left(\frac{\partial k}{\partial x_l}\frac{\partial\zeta}{\partial x_m}\right)\frac{\Omega_j}{\Omega^2} \\ &-2\frac{\beta_6\tau_{ij}\nu_t}{\rho k\nu}\Omega\Omega_i\Omega_j + \frac{\beta_7\zeta}{\Omega^2}\Omega_i\Omega_j S_{ij}\end{aligned} \tag{7}$$

where,

$$\tau_{ij} = 2\mu_t S_{ij} - \frac{2}{3}\rho k\delta_{ij}, \quad R_k = \frac{k}{\nu\sqrt{\zeta}}, \quad \nu_t = \frac{\mu_t}{\rho} \tag{8}$$

with μ_t being the eddy viscosity. The model constants are provided in Table 1.

Two departures from earlier modeling should be noted. First, when testing the model in a Navier-Stokes code, it was determined that the first term in equation 7 should be replaced by

$$-\frac{1}{\sigma_r}\frac{\partial\Omega_i}{\partial x_j}\left[\frac{\partial(\nu_t\Omega_i)}{\partial x_j} + \frac{\partial(\nu_t\Omega_j)}{\partial x_i}\right] \tag{9}$$

The original modeling was consistent with Taylor's vorticity transport theory [7]. However, we encountered similar difficulties here. The above modification removes the difficulty. It should be noted that, because of similarity considerations, the term under discussion did not contribute to the similarity equations employed in Ref. [1]. Therefore, the above modification does not change any of the model constants.

The second adjustment concerns the dissipation term in the ζ equation. The turbulent time scale $\frac{k}{\nu\zeta}$ can not be less than Kolmogorov's time scale. To allow for this result, the dissipation term now has the form

$$\frac{\beta_5\zeta^{\frac{3}{2}}}{R_k + \delta} \tag{10}$$

For the results presented here $\delta = 0.1$.

Results and Discussion

I. Attached Flows

For high turbulent Reynolds numbers, the eddy viscosity is chosen as

$$\nu_t = \frac{C_\mu k^2}{\nu\zeta} \quad , \quad C_\mu = 0.09 \tag{11}$$

For wall bounded flows the eddy viscosity and the turbulent Reynolds number are both zero at the wall. Because of this, the above expression is traditionally multiplied by the function f_μ. There is no unanimity on the form of f_μ in the near wall region [8]. More recent implementations such as that of Speziale et al [9] employ a function that depends on both Re_t and y^+ where

$$Re_t = \frac{k^2}{\nu^2\zeta} \quad , \quad y^+ = \frac{yU_\tau}{\nu} \quad , \quad U_\tau = \sqrt{\frac{\tau_w}{\rho}} \tag{12}$$

where τ_w is the wall shearing stress. Because separation may take place in the presence of adverse pressure gradients a different representation that does not require y^+ is employed. The resulting expression is given as

$$f_\mu = \min(f_\mu^*, 1.0),\ f_\mu^* = \left(1 + \frac{C_{\mu_1}}{Re_t^{\frac{3}{4}}}\right) \exp\left(\frac{-\sqrt{k}y}{\nu C_{\mu_2}}\right) \quad (13)$$

where

$$C_{\mu_1} = 4.0 \quad , \quad C_{\mu_2} = 40.0 \quad (14)$$

The boundary conditions for the two-equation model are

$$\begin{aligned} k_w &= 0 \\ k_\infty &= \frac{3}{2}(\mathcal{T}U_\infty)^2 \end{aligned} \quad (15)$$

and

$$\begin{aligned} \frac{\partial \zeta}{\partial y}|_w &= 0 \ , \ or \\ \frac{\partial}{\partial y}\left(\frac{1}{3}\frac{\partial k}{\partial y}\right) &= \zeta_w \ at\ y = 0 \end{aligned} \quad (16)$$

where $\mathcal{T}$ is the turbulent intensity ($\approx 1\%$) and ζ_∞ is determined by specifying a free stream ratio of $\frac{\mu_t}{\mu}|_\infty$ along with k_∞. The first boundary condition for ζ_w amounts to a simple extrapolation when a first order difference for $\frac{\partial \zeta}{\partial y}|_w$ is used. The second boundary condition for ζ is obtained by examining equation 6 in the near wall region. This equation is then used to solve for ζ_w as follows. First, we expand as a central difference

$$\zeta_w = \frac{\frac{\partial k}{\partial y}|_1 - \frac{\partial k}{\partial y}|_w}{3\Delta y}$$

where '1' represents the first point off of the wall and 'w' represents the wall. Since $k \sim y^2$ near the wall, we have

$$\frac{\partial k}{\partial y}|_w = 0 \quad (17)$$

and, therefore,

$$\zeta = \frac{k_1 - k_w}{3(\Delta y)^2} = \frac{k_1}{3(\Delta y)^2} \quad (18)$$

Using this boundary condition for ζ forces a $k \sim y^2$ variation near the wall. Results for both boundary conditions are presented for comparison.

There are a number of tests a turbulence model must meet to be considered a successful model. First, and foremost, it must predict the correct skin friction and pressure coefficients and other near wall measurements [8] of shearing stress, kinetic energy, and dissipation. Second, it must predict the correct growth rate, asymptotic shearing stress distribution, and velocity in the far wake. Finally, it must predict the correct 'B' constant that appears in the expression for the velocity in the log- law region, and the manner in which k varies with y in the near wall region [See Table 4.5 in Ref. [10]]. Recall that the correct near wall variation of k can be enforced through the use of the second boundary condition on ζ.

Figures 1- 3 show plots of k^+, ζ^+, and $\left(-\overline{\rho u'v'}\right)^+$ vs. y^+ in the near wall region where

$$k^+ = \frac{k}{U_\tau^2} \ , \ \zeta^+ = \frac{\zeta \nu^2}{U_\tau^4} \ , \ -\overline{\rho u'v'} = \frac{\tau_{1,2}}{U_\tau^2} \quad (19)$$

Also shown is the "average" of available data [8] together with the experimental measurements. The predictions compare well with the results summarized in Ref. [8] and experiments. It appears from Figure 1 that the peak k^+ is under predicted, nevertheless, it lies within the range of available experimental data ($k^+ \approx 2.8 - 6.0$). Figure 4 compares the calculated skin friction coefficient with the correlations of Cole and Schoenherr [11]. Again good agreement is indicated.

The constant 'B' in the log-law correlation

$$u^+ = \frac{1}{\kappa} ln y^+ + B \quad (20)$$

is typically 5. A plot of $y^+ - \frac{1}{\kappa}\ln y^+$ shows that 'B' is not exactly constant, but rather, varies slightly from approximately 4.4 to 5.2 over a y^+ ranging from 50 to 500.

The next set of figures compares calculated and measured wake data. Figures 5- 7 show a comparison of numerical, asymptotic, and experimental results for the defect velocity at the centerline, $\frac{U_e}{W_o}$ [U_e is the edge velocity, W_o is the centerline defect velocity], wake half width, b, and the maximum shear stress $\left(\frac{\tau}{W_o^2}\right)$, where τ is the shear stress, as a function of $\frac{x}{\theta}$ where θ is the momentum thickness. The asymptotic solution is that of the far wake with a constant eddy viscosity. The experimental results are obtained from Pot [12] and Weygandt and Mehta [13]. Again, good agreement is indicated.

Figures 8- 9 compare the defect velocity, W, and the shear stress distributions across the wake. Here, also good agreement with experiment [12, 14] is indicated.

The remaining figures show the Navier-Stokes (NS) solution for a NACA 0012 airfoil. All of the NS solutions were run using a third order upwind biased Roe scheme. Figure 10 shows the grid (301x101) which has an initial normal spacing of $1.e^{-6}\bar{C}$ and an outer boundary of $15\bar{C}$. Figures 11- 14 show the pressure and skin friction coefficients compared with the experimental data [15] and with the standard $k-\omega$ model of Wilcox [10]. The Wilcox model was chosen because it is widely known that this model gives good agreement with experiment for wall bounded flows.

Figures 11- 12 correspond to a Mach number of 0.502 and an angle of attack of 2.06 deg. Once again, good agreement for both C_p and C_{fe} are shown. For this case, the choice of boundary condition on ζ affects the numerical stability of the solution by reducing oscillations

around the trailing edge. Except for this small region around the trailing edge, the choice of boundary condition has very little effect on the solution. This insensitivity was also noted when examining the flat plate boundary layer solution. The reason for this insensitivity is seen by noting that for a flat plate, the k-ζ model (with simple extrapolation for ζ), produces a $k \sim y^2$ behavior near the wall. Therefore, using the second boundary condition to impose a y^2 variation should have no effect.

The next case (Mach=0.80, $\alpha = 0.0$) examines the behavior of the k-ζ turbulence model for a transonic airfoil. From figure 14, it is noted that an extrapolation boundary condition for ζ causes a large spike in the skin friction. This oscillation is eliminated by imposing the second bc for ζ. Therefore, it appears that bc2 is the appropriate choice for a boundary condition for non-simple flow fields. When using bc2, good agreement with the k-ω model is shown. This boundary condition was used in calculating separated flows.

II. Separated Flows

It is a known fact that both k-ω and k-ϵ models are, in general, unable to predict separated flows [16]. In a recent investigation, Rao and Hassan [16] showed that the reason for this behavior is a result of inadequate modeling of the diffusion term in the k-equation. There are two ways of modifying the diffusion term: one by remodeling it, which is the approach followed in Ref. [16]; the other by adjusting the model 'constant' in the diffusion term. Because subsonic and supersonic boundary layers behave differently in the presence of adverse pressure gradients it has not been possible to remodel the diffusion term in such a way so as to accommodate both subsonic and supersonic flows. As a result, the second approach, which entails adjusting the model constant, was employed here.

The approach presented here is tentative because it does not have the desired general form. It entails adjusting $\frac{1}{\sigma_k}$ in the turbulent kinetic energy equation by subtracting from it a dimensionless pressure gradient parameter. A number of guidelines were set for selecting such a parameter. It may be recalled that boundary layer theory is rich with such parameters, unfortunately, most of them are not convenient to compute in a Navier-Stokes solver. Moreover, it is desirable to avoid quantities that require a search in the flow field. Further, the new model should be such that it has little or no effect on the attached flow cases discussed above. Finally, the model must be able to handle a difficult separated flow situation like the NACA 0012 at $\alpha = 2.26$ and $M_\infty = 0.8$.

In the proposed model, $\frac{1}{\sigma_k}$ in the k-equation is replaced by

$$\frac{1}{\sigma_k} - \beta_t \tag{21}$$

where

$$\beta_t = \frac{x}{q_\infty}\frac{\partial P}{\partial S} \quad , \quad q_\infty = \frac{1}{2}\rho_\infty U_\infty^2 \tag{22}$$

and

$$0 < \beta_t < 1.4 \tag{23}$$

It was necessary to limit β_t because the term has a large spike around the shock. Note that when $\frac{\partial P}{\partial S} = 0$, the original model constants are recovered.

The above model was used to calculate the flow past an NACA 0012 at $\alpha = 2.26$ and $M_\infty = 0.79$. The results are shown in Figures 15 and 16, and compared with a calculation by Rumsey and Anderson [17] using the Johnson and King model, and a k-ω model. Figure 15 compares the pressure distribution while Figure 16 compares the skin friction. The present and Johnson and King give good agreement with experiment, but the k-ω does not. Unfortunately, a lack of experimental data does not permit a meaningful discussion of skin friction results.

Conclusions

From the results indicated here, it has been shown that the model developed in Ref. [1] can be used for both wall bounded and free shear flows using one set of model constants. It has also been shown that the model can be easily incorporated into either a boundary layer or Navier-Stokes code. Finally, it has been demonstrated that the second boundary condition for enstrophy is more accurate for non-simple flow fields. We recognize that, although the tentative diffusion model presented here is a good start, a more general model is required. Moreover, additional validations would be desirable especially for separated flows.

Acknowledgments

This work is supported in part by the following grants: NASA Grant NAG-1-244, and the Mars Mission Research Center funded by NASA Grant NAGW-1331. The authors would like to express appreciation to the North Carolina Super Computing Center for use of these facilities.

References

[1] Robinson, D.F., Harris, J.E., and Hassan, H.A. "A Unified Turbulence Closure Model for Axisymmetric and Planar Free Shear Flows". AIAA Paper 95-0360, January 1995.

[2] Tennekes, H., and Lumley, J.L. *"A First Course in Turbulence"*. The MIT Press., Cambridge, MA, 1989.

[3] Harris, J.E., and Blanchard, D.K. "Computer Program for Solving Laminar, Transitional, or Turbulent Compressible Boundary-Layer Equations for Two-Dimensional and Axisymmetric Flow". NASA TM 83207, NASA Langley, Feb 1982.

[4] Gaffney, R.L., Salas, M.D., and Hassan, H.A. "An Abbreviated Reynolds Stress Turbulence Model for Airfoil Flows". AIAA Paper 90-1468, June 1990.

[5] Holst, Terry L. "Viscous Transonic Airfoil Workshop Compendium of Results". *Journal of Aircraft*, Vol. 25, No. 12:1073–1087, December 1988.

[6] Johnson, D.A., and King, L.S. "A Mathematically Simple Closure Model for Attached and Separated Turbulent Boundary Layers". *AIAA Journal*, Vol. 23, No. 11:1684–1692, November 1985.

[7] Taylor, G.I.,. "Distribution of Velocity and Temperature between Concentric Rotating Cylinders". *Proceedings of the Royal Society of London*, Ser. A, Vol. 151, No. A874:494–512, October 1935.

[8] Patel, V.C., Rodi, W., and Scheuerer, G. "Turbulence Models for Near-Wall and Low Reynolds Number Flows: A Review". *AIAA Journal*, Vol. 23, No. 9:1308–1319, July 1982.

[9] Speziale, C. G., Abid, R., and Anderson, E.C. "Critical Evaluation of Two-Equation Models for Near-Wall Turbulence". *AIAA Journal*, Vol. 30, No. 2:324–331, Feb 1992.

[10] Wilcox, D. C. *"Turbulence Modeling for CFD"*. DCW Industries, Inc., La Canada, CA, 1993.

[11] Schetz, J. A. *"Foundations of Boundary Layer Theory for Momentum, Heat, and Mass Transfer"*. Prentice-Hall, Nov. 1984.

[12] Pot, P.J. "Measurement in a Two-Dimensional Wake and in a Two-Dimensional Wake Merging into a Boundary Layer". Data Report NLR TR-79063 U, the Netherlands, 1979.

[13] Weygandt, J.H., and Mehta, R.D. "Asymptotic Behavior of a Flat Plate Wake". NASA CR-185917, 1989.

[14] Ramaprian, B.R., Patel, V.C., and Sastry, M.S. "The Symmetric Turbulent Wake of a Flat Plate". *AIAA Journal*, Vol. 20, No. 9:1228–1235, Sept 1982.

[15] Thibert, J.J., and Granjacques, M., and Ohman, L.H. "Experimental Data Base for Computer Program Assessment". NACA 0012 Airfoil, AGARD Advisory Report No. 138, May 1979.

[16] Rao, M.S., and Hassan, H.A. "Modeling of Turbulence in the Presence of Adverse Pressure Gradients". AIAA Paper 96-2429, AIAA 14th Applied Aerodynamic Conference, June 1996.

[17] Rumsey, Christopher L., and Anderson, W. Kyle. "Parametric Study of Grid Size, Time Step, and Turbulence Modeling on Navier-Stokes Computations Over Airfoils". *AGARD 62nd Meeting of the Fluid Dynamics Panel Symposium on Validation of Computational Fluid Dynamics*, Paper No. 5, May 1988, Lisbon, Portugal.

Table 1: Turbulence Model Closure Coefficients

Constants	$k-\zeta$
C_μ	0.09
κ	0.40
α_3	0.35
β_4	0.42
β_5	2.37
β_6	0.10
β_7	0.75
β_8	2.30
σ_r	2.00
$\frac{1}{\sigma_k}$	1.80
$\frac{1}{\sigma_\zeta}$	1.46

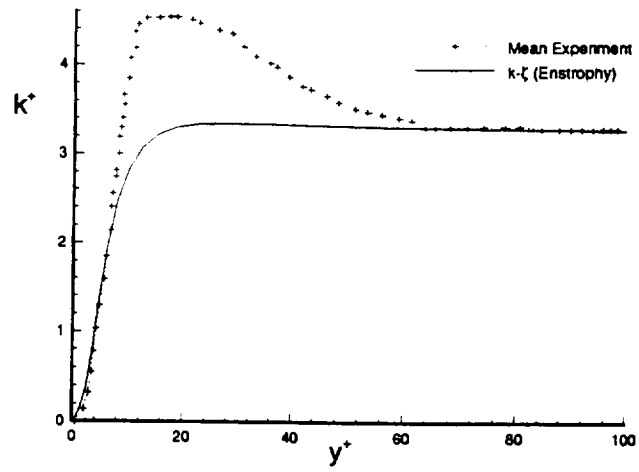

Figure 1: Near Wall Behavior of Turbulent Kinetic Energy (Flat Plate)

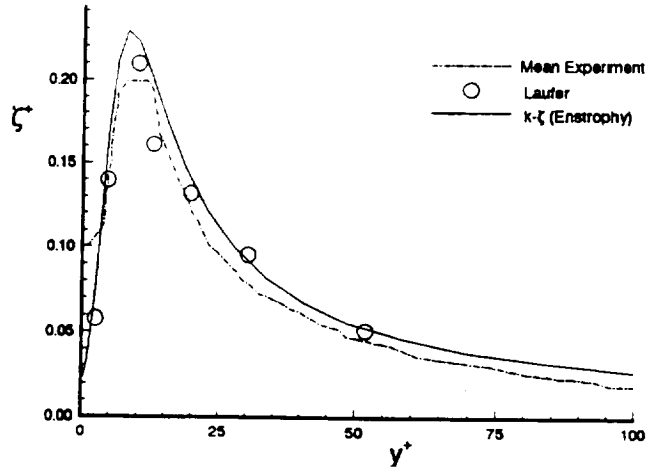

Figure 2: Near Wall Behavior of Enstrophy (Flat Plate)

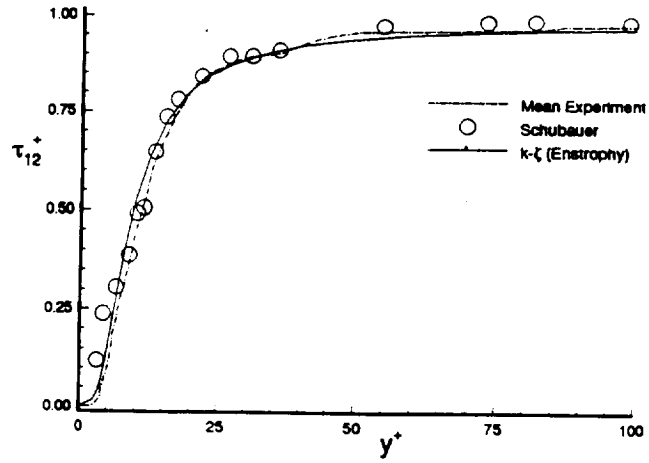

Figure 3: Near Wall Behavior of Reynolds Stress (Flat Plate)

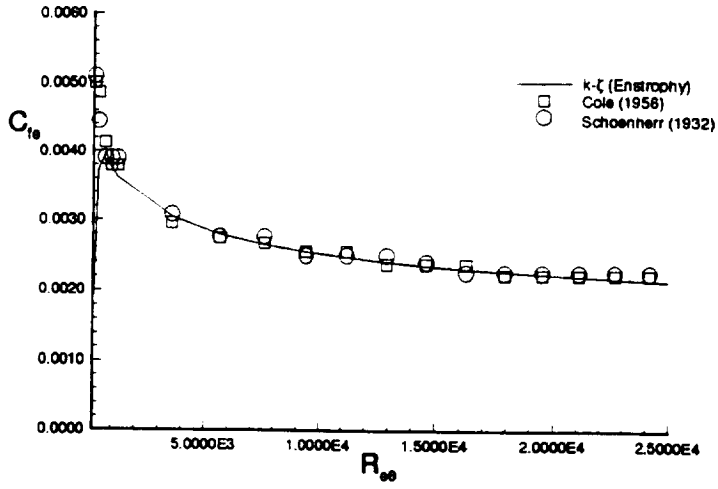

Figure 4: Skin Friction Coefficient (Flat Plate)

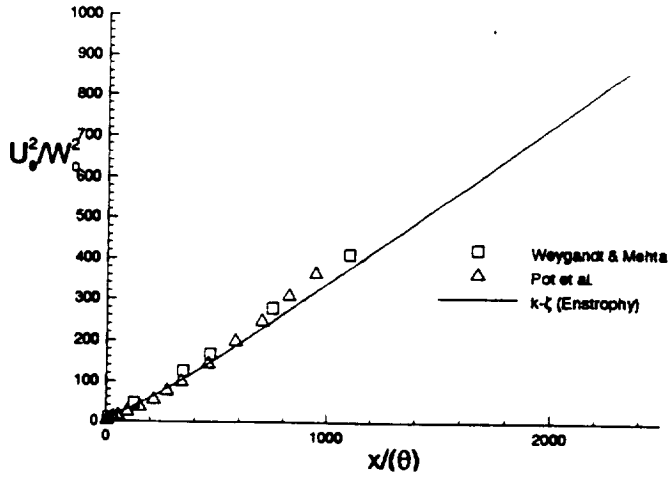

Figure 5: Streamwise Variation of Maximum Velocity Defect

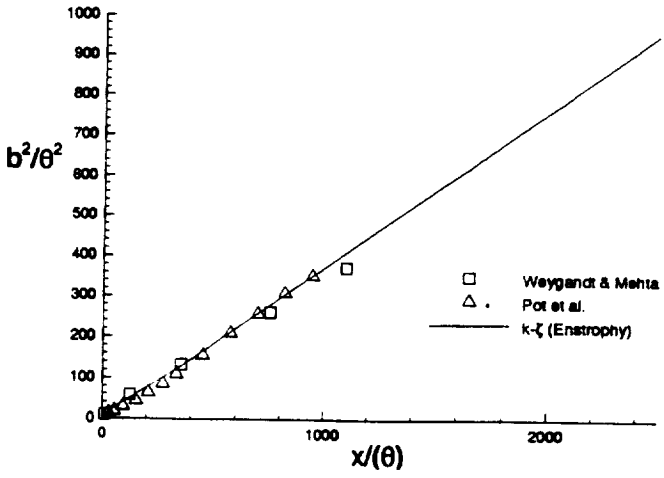

Figure 6: Streamwise Variation of Wake Half Width

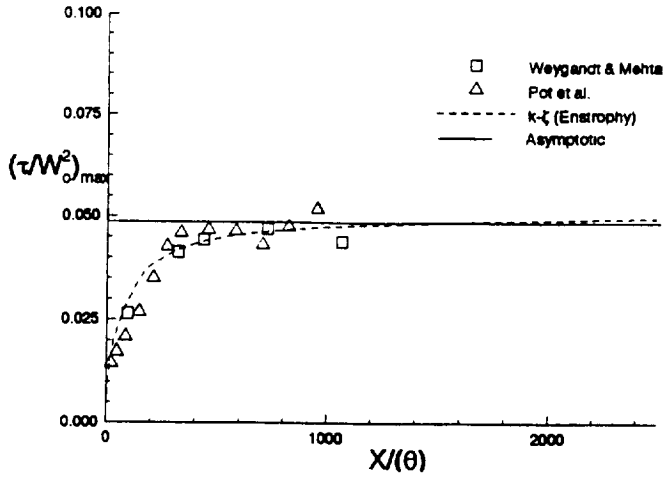

Figure 7: Streamwise Variation of Maximum Shear Stress

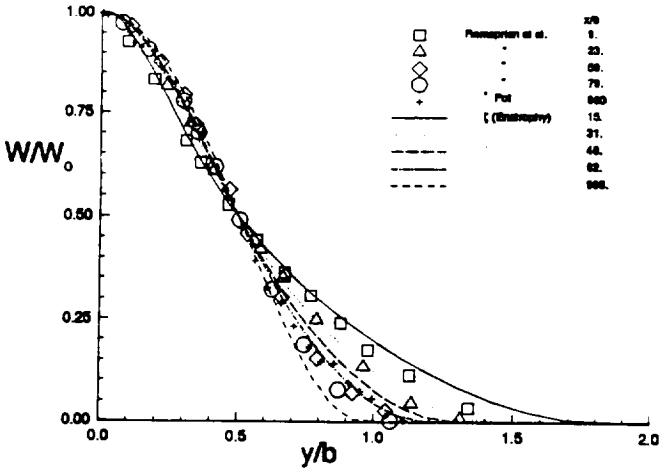

Figure 8: Wake Velocity-Defect Profiles

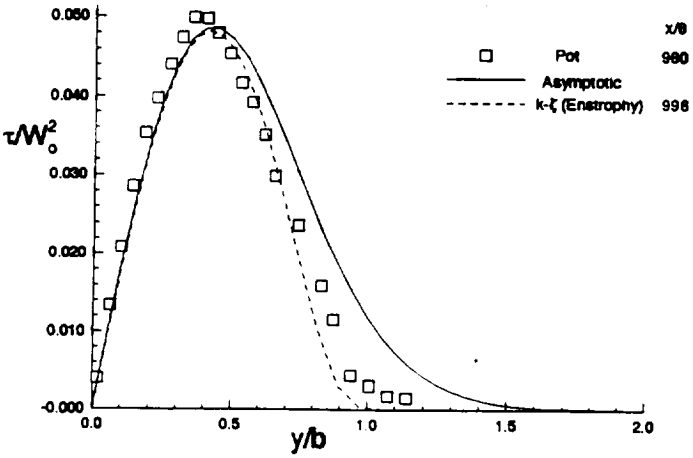

Figure 9: Wake Shear Stress Profiles

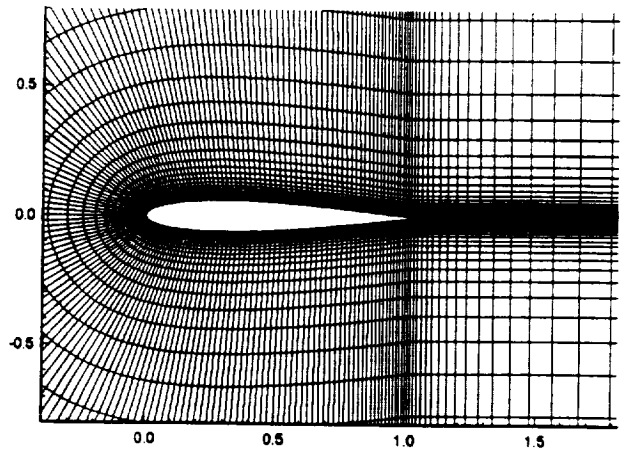

Figure 10: Partial View of C-mesh for NACA 0012 Airfoil

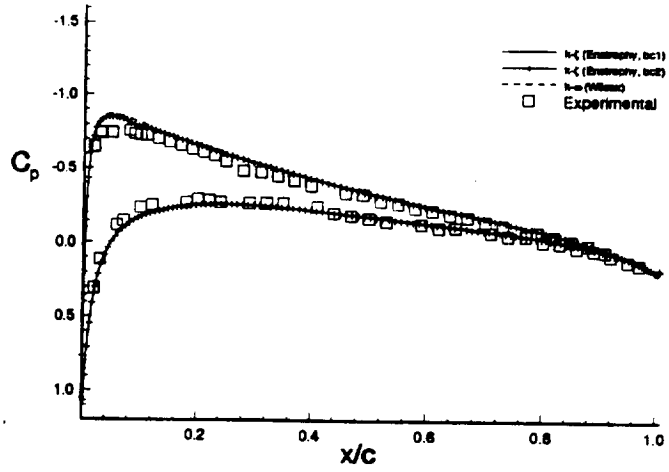

Figure 11: Pressure Distribution for NACA 0012 Airfoil ($M_\infty = .502, Re_\infty = 2.91e6, \alpha = 2.06$)

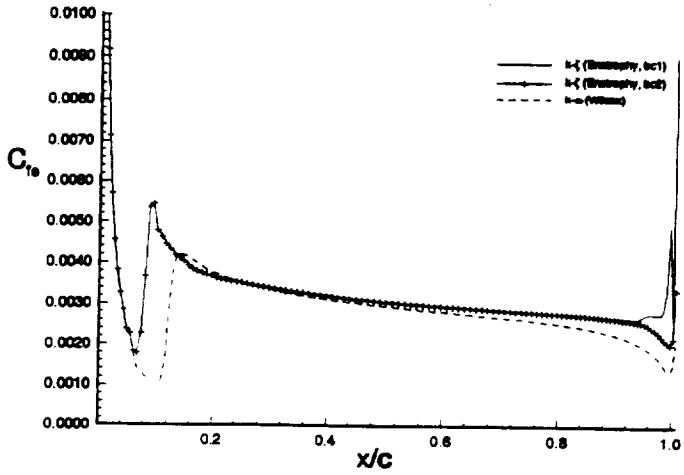

Figure 12: Skin Friction Comparison for NACA 0012 Airfoil ($M_\infty = .502, Re_\infty = 2.91e6, \alpha = 2.06$)

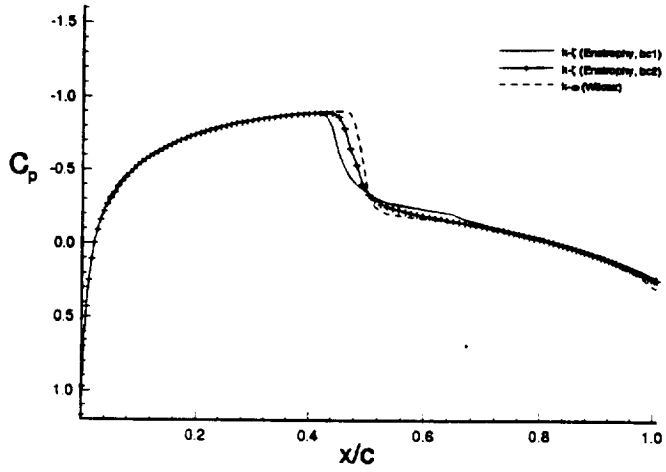

Figure 13: Pressure Distribution for NACA 0012 Airfoil ($M_\infty = 0.8, Re_\infty = 9.0e6, \alpha = 0.0$)

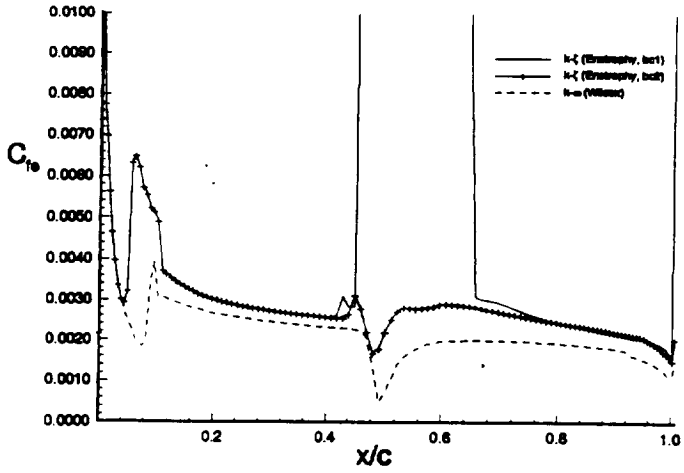

Figure 14: Skin Friction Comparison for NACA 0012 Airfoil ($M_\infty = 0.8, Re_\infty = 9.0e6, \alpha = 0.0$)

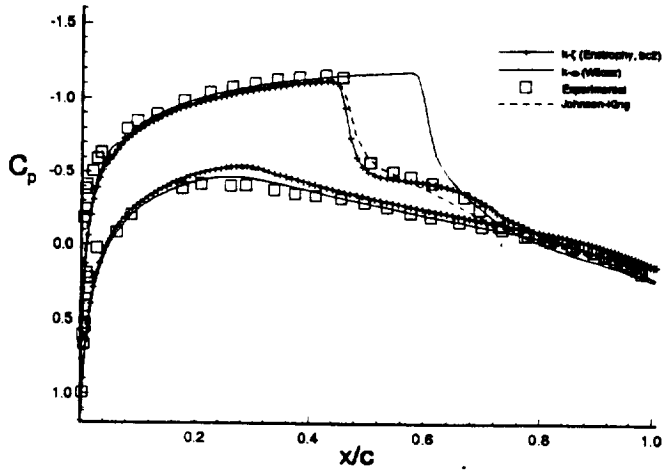

Figure 15: Pressure Distribution for NACA 0012 Airfoil ($M_\infty = 0.799, Re_\infty = 9.0e6, \alpha = 2.26$)

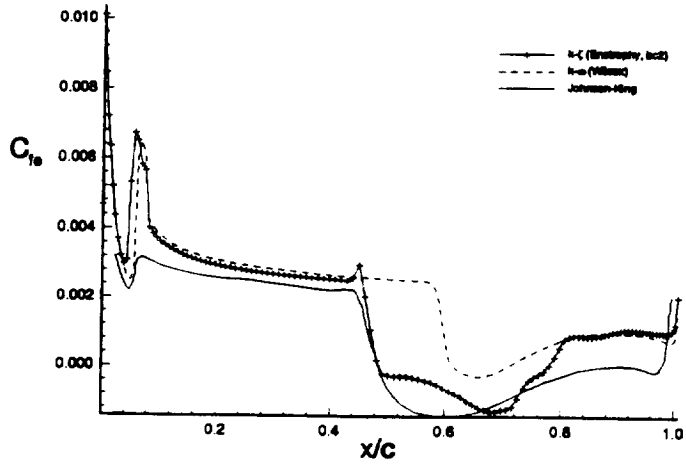

Figure 16: Skin Friction Comparison for NACA 0012 Airfoil ($M_\infty = 0.799, Re_\infty = 9.0e6, \alpha = 2.26$)